Norwegian Meteorological Institute
met.no

met.no report

no. 7/2010
Climate

A Study of Storms and Winds in the North-Atlantic

R.E. Benestad

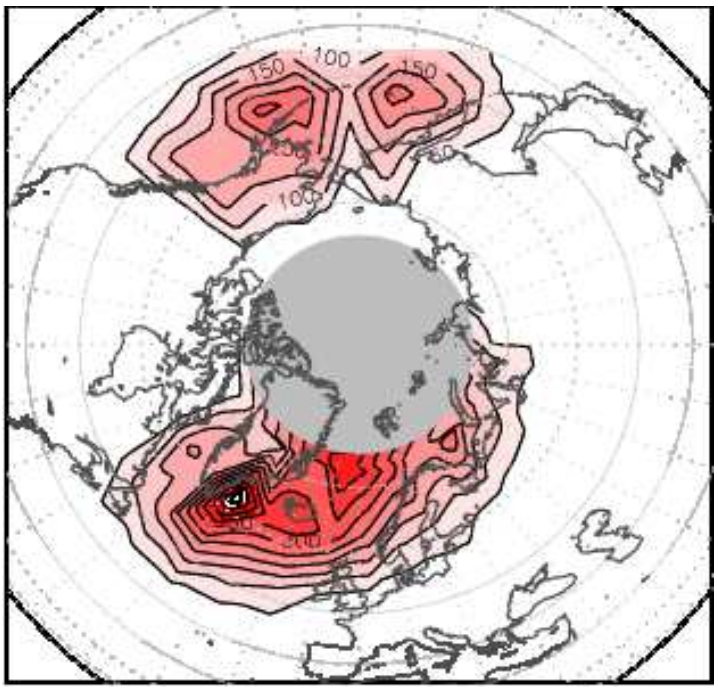

Norwegian Meteorological Institute
met.no

report

Title	Date
A Study of Storms and Winds in the North-Atlantic	August 11, 2010
Section	**Report no.**
Climate	7/2010
Author	**Classification**
R.E. Benestad	● Free ○ Restricted
	ISSN 1503-8025
	e-ISSN 1503-8025
Client(s)	**Client's reference**
CES & met.no	

Abstract

Storm statistics are derived from mean sea level pressure observations, re-analyses, and regional climate model results, based on geostrophic wind analysis and a calculus-based identification method. The analysis yields storm counts for events with central pressure below a set of given threshold values, in addition to estimates of the maximum gradient wind speed, spatial extent, and geographical distribution. An evaluation is performed in terms of a comparison with similar analysis based on re-analysis results and station observations of mean sea level pressure. The main conclusion from this study is that no significant trends at the 5% level were found in the maximum gradient winds over the period (1950–2050) simulated by the regional climate model following the SRES A1b emission scenario, but the model results had a bias compared to similar analysis based on observations or re-analysis data. There were indications of long-term increases in the frequency for the strongest storms in a 20th century re-analysis data set. The 20th century re-analysis data also suggested a decrease in the maximum gradient winds over 1891–2008. However, there is a concern that the mean sea level pressure fields in the re-analysis products are not homogeneous and that regional climate models with a small domain are too constrained by the driving models, thus yielding too smooth spatial structures.

Keywords

Cyclones, wind speed, trend analysis, regional climate models

Disciplinary signature	Responsible signature
Inger Hanssen-Bauer	Eirik Førland
Inger Hanssen-Bauer	Eirik Førland

Postal address P.O Box 43 Blinde rn N-0313 OSLO Norway | **Office** Niels Henrik Abel s vei 40 | **Telephone** +47 2296 3000 | **Telefax** +47 2296 3050 | **e-mail:** met.inst@met.no **Internet:** met.no | **Bank account** 7694 05 00601 | **Swift code** DNBANOKK

Contents

1 Introduction

Storms represent one type of extremes that can have dramatic influence on society and ecosystems, through damages caused by strong winds, storm surges or precipitation. In this context, the term 'storm' will refer to mid-latitude cyclones, characterised by local minima in the sea level pressure fields, strong pressure gradients, high vorticity, and high winds. Mid-latitude storms are also referred to as low-pressure systems.

1.1 Motivation

One motivation for analysing trends in storminess is from a practical point of view: the question whether changes in the intensity or frequency of storms will affect the society in many ways. From an energy production perspective, storms can affect the operation of wind generators, wave heights, or rainfall patterns. Changes in the storm track climatology - a plausible consequence of a climate change - will potentially affect the utility of power production installations.

There are also scientific reasons why changes in storm statistics is interesting. They involve large eddy flow which affect the meridional transport of heat, momentum, and mass, and hence play a role for the planetary climate system. Large-scale dynamics form the core of mid-latitude storms, which furthermore differ from tropical cyclones where thermodynamics are believed to play a greater role (the concept of heat engines are more appropriate for tropical cyclones).

Storms and the deepening of low-pressure systems involve some mechanism of 'instability' that is responsible of a growing disturbance. The type of instability may be based on pure dynamics, such as 'baroclinic instability' (*Gill*, 1982; *Fleagle & Businger*, 1980; *Houghton*, 1991; *Lindzen*, 1990), or may involve thermodynamics (cloud formation and condensation). A necessary condition for barotropic instabilities to arise is that:

$$\beta - \frac{d^2U}{dy^2} < 0, \tag{1}$$

where $\beta = df/dy$, $f = 2\omega\sin(\phi)$ (s^{-1}) is the Coriolis parameter, y is north-south coordinate (m), and U is the zonal flow (m/s).

2 Method

The spatial gradients in the mean sea-level pressure (SLP) can be related to the winds through the geostrophic wind equation (*Gill*, 1982):

$$v_g(\phi) = \frac{1}{f(\phi)\rho}\sqrt{(\partial p/\partial y)^2 + (\partial p/\partial x)^2}. \tag{2}$$

The parameters ϕ is the latitude (radians), the Coriolis parameter $f(\phi) = 1.47\sin(\phi)\times 10^{-4}$ (s^{-1}), density $\rho = 1.25$ (kgm^{-3}), x is east–west distance (m), and y north–south distance (m). The 'gradient wind' (*Fleagle & Businger*, 1980) yields a more representative estimate of winds around low-pressure systems at a radius r (m) than the geostrophic wind equation, and can be estimated according to the expression:

$$V(\phi) = -\frac{1}{2f(\phi)r}[1 \pm \sqrt{1 + \frac{4v_g(\phi)}{f(\phi)r}}]. \quad (3)$$

Storm systems were identified from gridded SLP fields (maps) using the calculus cyclone identification (CCI) method proposed by *Benestad & Chen* (2006). The CCI analysis provided estimates of the position and time of the storms in addition to their central pressure, spatial extent, maximum gradient wind, and pressure gradients. An example of some diagnostics from this method are shown in Figure 1.

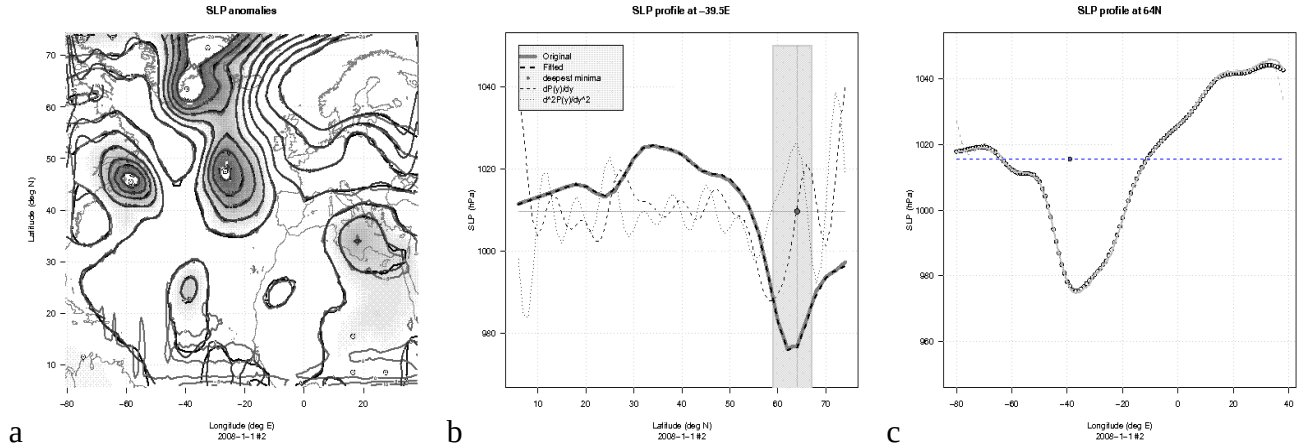

a b c

Figure 1: *Example showing some diagnostics from CCI. Panel (a) shows a SLP map where the local minima identified by CCI are marked with circular symbols. Panel (b) shows a north-south SLP profile, and a highlight of the deepest SLP minimum. Also shown are the approximation based on a truncated Fourier series ('fitted'), and the first and second derivatives (re-scaled for plotting). The shaded area shows the area between the points of inflexion ($d^2(SLP)/dy^2 = 0$) defining the storm radius, and the symbol marks the position of its centre. Right panel shows a similar but simpler diagnostic for the east-west SLP profile.*

It is also possible to derive statistics on storm systems from three station measurements of mean sea level pressure (p_1, p_2, and p_3) through stations making up triangles proposed by *Alexandersson* et al. (1998, 2000) (henceforth referred to as "triangulation", also discussed in a more recent study by *Wern & Bärring* (2009)):

$$\begin{aligned} a &= \frac{(p_3 - p_1) - y_3(p_2 - p_1)/y_2}{x_3 - x_2 y_3/y_2} \\ b &= \frac{p_2 - p_1 - a x_2}{y_2} \\ u_g &= -\frac{b}{f\rho} \\ v_g &= \frac{a}{f\rho}. \end{aligned} \quad (4)$$

The variables y_2 and x_2 represent the north–south and east–west distance (m) between first and second stations whereas y_3 and x_3 are the corresponding distances between first and third

stations (here using mean value for the Coriolis parameter $f = 1.25 \times 10^{-4} s^{-1}$). The coefficients a and b are convenient temporary variables used to aid the calculations, and u_g and v_g represent the zonal and meridional components of the geostrophic wind respectively.

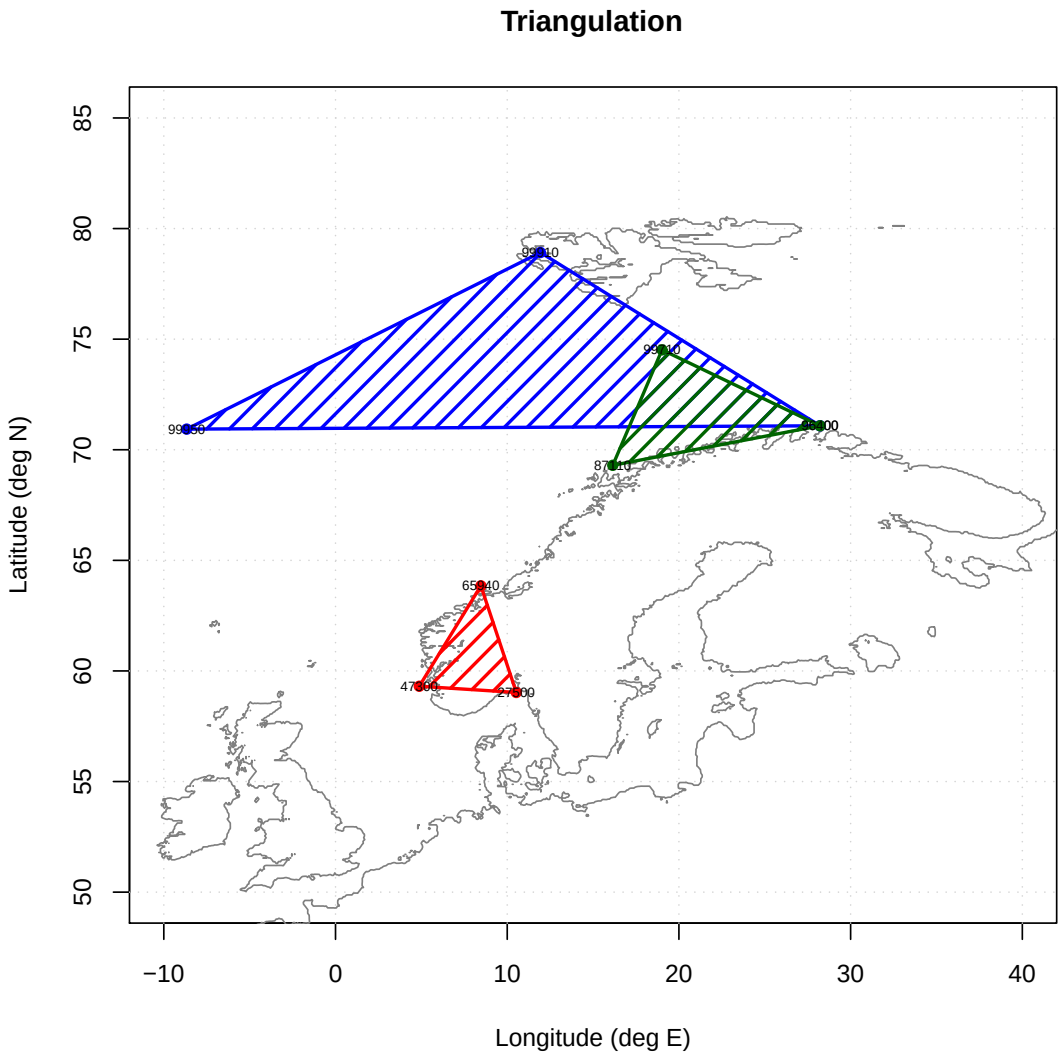

Figure 2: *Map showing the location of the stations used in wind estimation based on triangulation as well the triangles used. Here, the red triangle represent UTSIRA FYR (47300), FÆRDER FYR (27500), and SULA (65940). Blue triangle: JAN MAYEN (99950), NY-ÅLESUND (99910), and SLETTNES FYR (96400). Green triangle: ANDØYA (87110), BJØRNØYA (99710), and SLETTNES FYR (96400). Here the numbers in parentheses are the station number.*

Figure 2 shows a map of the stations used for triangulation. The corresponding analyses performed for RCM and GCM values were based on simulated SLP interpolated to the same coordinates as the stations.

Table 1: *The station data ("observations" at 12:00) used from the climate archive of the Norwegian Meteorological Institute, providing the basis for the triangles shown in Figure 2. The element is "PR" (pressure at mean sea level) extracted with the R-call KDVH from the R-package the met.no.REB (version 1.2-5).*

Name	Station number	Longitude	Latitude	Altitude (m.a.s.l.)	Interval	N
ANDØYA	87110	16.1467°E	69.2967°N	10	1958–2009	17331
BJØRNØYA	99710	19.0167°E	74.5167°N	16	1956–2009	19627
SLETTNES FYR	96400	28.2178°E	71.084°N	8	1957–2005	17640
JAN MAYEN	99950	8.6667°W	70.9333°N	10	1922–2006	30437
NY-ÅLESUND	99910	11.9333°E	78.9167°N	8	1974–2006	11461
UTSIRA FYR	47300	4.8783°E	59.3077°N	55	1957–2006	17860
FÆRDER FYR	27500	10.53°E	59.0267°N	6	1957–2006	17915
SULA	65940	8.4667°E	63.8467°N	5	1975–2005	9751

3 Data

Here 'ENSEMBLES' refers to the simulation by the Norwegian HIRHAM model (*Haugen & Ødegaard*, 2003) used in the ENSEMBLES project (*van der Linden & Mitchell*, 2009) to produce simulations of the regional climate, spanning over the 1950–2050 interval.

Only a limited part of the ENSEMBLES results were analysed (the met.no HIRHAM only), as instantaneous mean sea-level pressure (SLP) was not saved in the standard archive of ENSEMBLES. Rather, only the *surface pressure* was saved, but estimating SLP from the surface pressure over land with varying altitude and temperature is not quick and straight forward. The analysis presented here represent vast quantities of data, and computing SLP from the surface pressure would require more resources than was available for the task of cyclone analysis in this project.

The RCM data were saved in a rotated coordinate system, and had to be re-gridded in a regular longitude-latitude before calculus-based cyclone identification (*Benestad & Chen*, 2006, CCI) could be applied. The large volume of data and computer memory limitation inhibited fast processing, as the data had to be read piecewise (due to memory limitations) and a bilinear interpolation was done sequentially in `R` (*Ihaka & Gentleman*, 1996). A recommendation for the future would be to archive such data in longitude-latitude format to allow fast processing of the data (e.g. using the NOAA/PMEL analysis tool *Ferret*).

The analysis also involved SLP from a selection of stations in the station network. These were taken from the climate archives of the Norwegian Meteorological Institute ('http://eKlima.met.no' - see Table 1), and represent the observations in the triangulation analysis shown in Figure 2, although interpolated values from climate models were also used.

The triangulation and CCI analyses of the RCM results will be biased if the points are near the lateral boundary of the RCM domain where the SLP is distorted. This distortion is largely due to the interpolation routine `akima`, which does not accept missing values. Instead, missing values were replaced with -99 before the interpolation, and all values lower than 900 (hPa) were set to missing after the interpolation. Figure 3 of RCM SLP shows distortions near the boundaries. It is also evident that the region corresponding to this domain excluded many of

the stations used in the triangulation study (Figure 2 & Table 1). The black rectangle in the map shows the region with data extracted - it was chosen to be the largest region that gave valid data for all grid boxes, yet avoided the boundaries with distorted values for SLP.

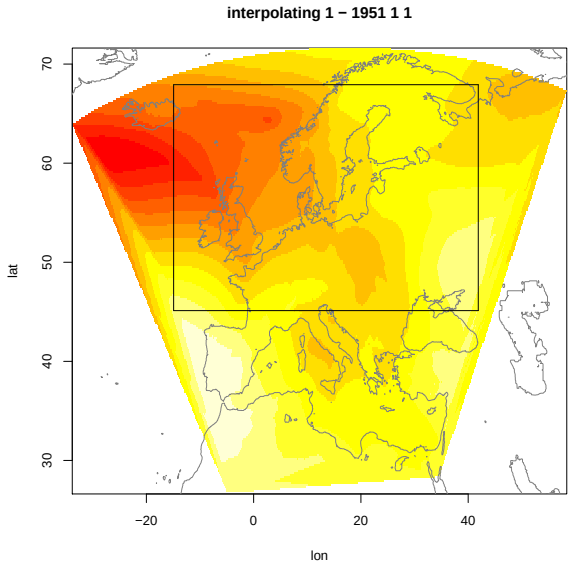

Figure 3: *A snapshot of the RCM SLP field, showing distortions near the lateral boundaries after the fields have been interpolated onto a regular longitude-latitude grid.*

A number of RCM results were also taken from the PRUDENCE project (*Déqué* et al., 2007)[1]. These are listed in Table 2. Note that some of the RCM domains did not include the Artic stations used in the blue triangle. In addition to the RCM data, a set of SLP fields was taken from a GCM ECHAM5 (*Solomon* et al., 2007) following the SRES A1b emission scenario for the interval 01.01.2046–31.12.2065. The analyses based on GCM results were mainly used to provide a reference for the RCM-based analyses.

Instantaneous SLP fields at 6 hr intervals were taken from the ERA interim (*Simmons* et al., 2007) re-analysis (ERAINT) covering the period 01.01.1989–31.03.2009. Furthermore, a 20th century re-analysis (1891–2008) (*Compo* et al., in preparation) available from http://www.esrl.noaa.gov/[2] was used to analyse the storm statistics for longer historical periods. The SLP fields from the 20th century re-analysis were also available at 6 hr intervals. The RCM results from the ENSEMBLES too were provided with 6 hr intervals, while all the PRUDENCE data (Norwegian HIRHAM, Danish HIRHAM, Danish HIRHAM) and ECHAM5 data were stored at 24 hr intervals.

[1] http://prudence.dmi.dk/

[2] http://www.esrl.noaa.gov/psd/data/gridded/data.20thC_Rean.htm

Table 2: *List of RCMs used in the triangulation analysis. 'Ctl' refers to the control integration and 'SRES A2' and SRES B2' refer to the 'Special Report Emission Scenario' A2 or B2 as described in* Solomon *et al. (2007) for the interval 2071–2100 (The RCM year was 360 days). The Ctl runs were performed for 1961–1990.*

RCM	GCM	Scenario	Project	Centre
Norwegian HIRHAM	HadAM3H	Ctl	PRUDENCE	met.no
Norwegian HIRHAM	HadAM3H	SRES A2	PRUDENCE	met.no
Norwegian HIRHAM	HadAM3H	SRES B2	PRUDENCE	met.no
Danish HIRHAM	ECHAM4	Ctl	PRUDENCE	DMI
Danish HIRHAM	ECHAM4	SRES A2	PRUDENCE	DMI
Danish HIRHAM	ECHAM4	SRES B2	PRUDENCE	DMI
RCAO	HadAM3H	Ctl	PRUDENCE	SMHI
RCAO	HadAM3H	SRES A2	PRUDENCE	SMHI
RCAO.22	HadAM3H	SRES A2	PRUDENCE	SMHI
Norwegian HIRHAM	HadAM3H	SRES A1b	ENSEMBLES	met.no

4 Results

4.1 Evaluation - southern Norway

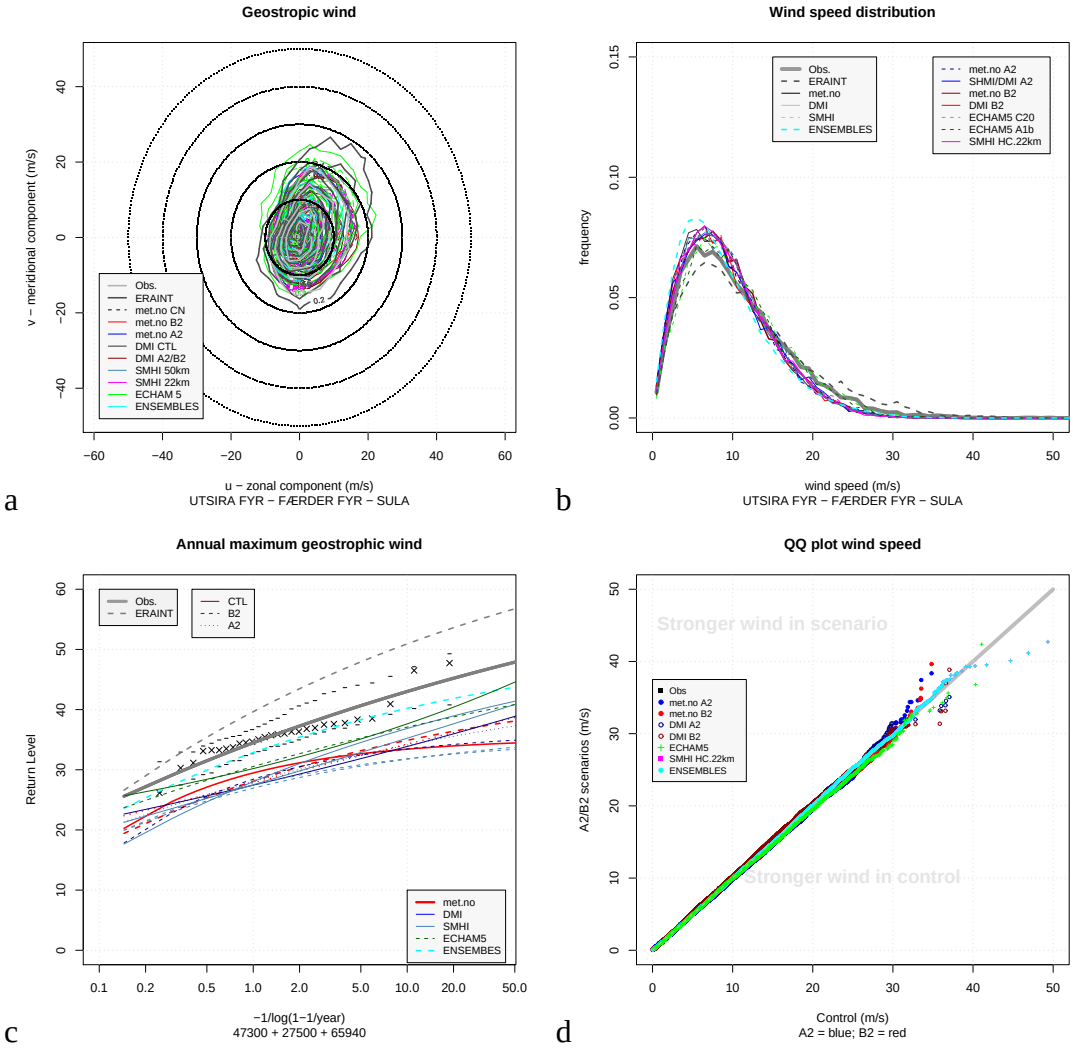

Figure 4: *Various geostrophic wind statistics derived from SLP. Here the geostrophic wind estimated through triangulation (Utsira fyr, Ferder fyr, & Sula) as well as a number of climate models (a). Panel b shows the statistical distribution of the wind speed, and panel c shows corresponding return-level analysis. Panel d shows a qq-plot of simulated wind speeds for the past versus the future. Note, the ENSEMBLES results shown here span 1950–2020, the RCMs span 2071–2100, ERAINT spans 1989–2009, while the observations cover the intervals stated in Table* **??**

Figure 4 shows wind statistics for the red triangle in Figure 2 - wind analysis over southern Norway (over land rather than over sea). All the wind estimates derived from the regional and global climate models suggest similar wind speeds as estimated from the barometric observations at Utsira fyr, Ferder fyr, and Sula. There is a reasonable agreement between model results and SLP observations, however, the extreme wind analysis (panel c) suggests higher return-levels in the observations than the PRUDENCE RCMs, due to a fatter upper tail in the observations (panel b). The ENSEMBLE results and the return value analysis based on ECHAM5,

however, exhibited better agreements with the observations and ERAINT.

There is no systematic or unambiguous tendency regarding the wind strength of the past compared with the future according to the qq-plot shown in panel d.

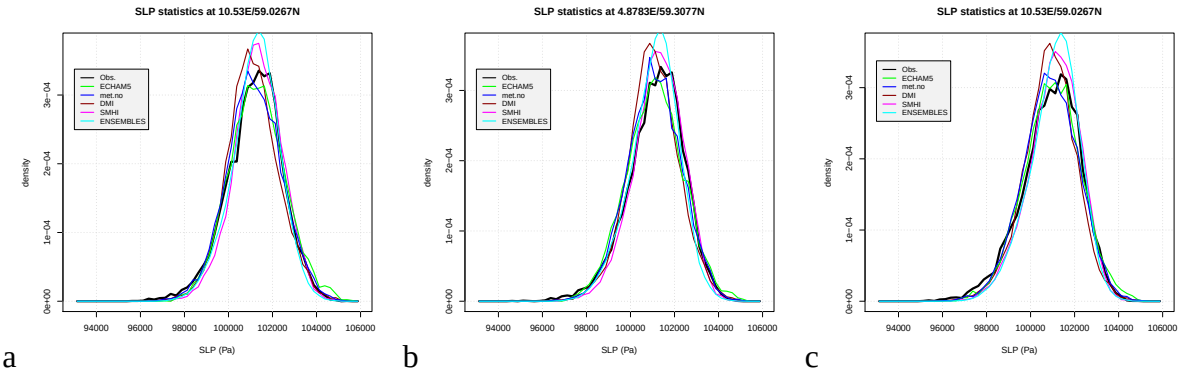

Figure 5: *Statistical distribution of the SLP used to estimate the wind statistics in Figure 4 for southern Norway. The three panels represent stations 27500 (Ferder fyr; left), 47300 (Utsira fyr; middle), and 65940 (Sula; right) respectively.*

Figure 5 shows histograms of the SLP for the three locations used in the red triangle in Figure 2. All the climate models exhibit a similar spread.

4.2 Evaluation - northern Norway

The wind statistics for northern Norway, shown in Figures 6–7, only provide results for the Norwegian HIRHAM from the PRUDENCE project. The other RCMs used domains that did not cover all the locations used in the triangulation (green triangle in Figure 2). The two PRUDENCE RCMs (HIRHAM A2 & B2, driven by HadAM3H) exhibit systematic biases in the wind directions and magnitude, while the ECHAM5 GCM returned magnitudes similar to the observations and ERAINT.

The HIRHAM A2 & B2 PRUDENCE indicate higher return-levels than the observations (panel c) as well as a tendency of weakening of high wind speeds in the future (values below the diagonal in panel d). The biases in the wind speeds were most likely due to systematic shifts in the statistical distribution of the model results for the mean sea-level pressure at Andøya and Slettnes fyr (Figure 7).

4.3 Evaluation - the Svalbard region

Figures 8–9 show a similar analysis for the Arctic region (blue triangle in Figure 2). The wind estimates from HIRHAM from the PRUDENCE project (the only RCM to include the locations of the Arctic triangle) were unrealistic - with too strong wind speeds. Since the other RCMs did not have valid data for these locations, it is not possible to say whether these would give a better description. However, the GCM was in good agreement with the observations. All the PRUDENCE RCMs also tend to give surprisingly similar results in terms of statistics for southern Norway, and there is no particular reason suggesting that they would not give similar results at higher latitudes.

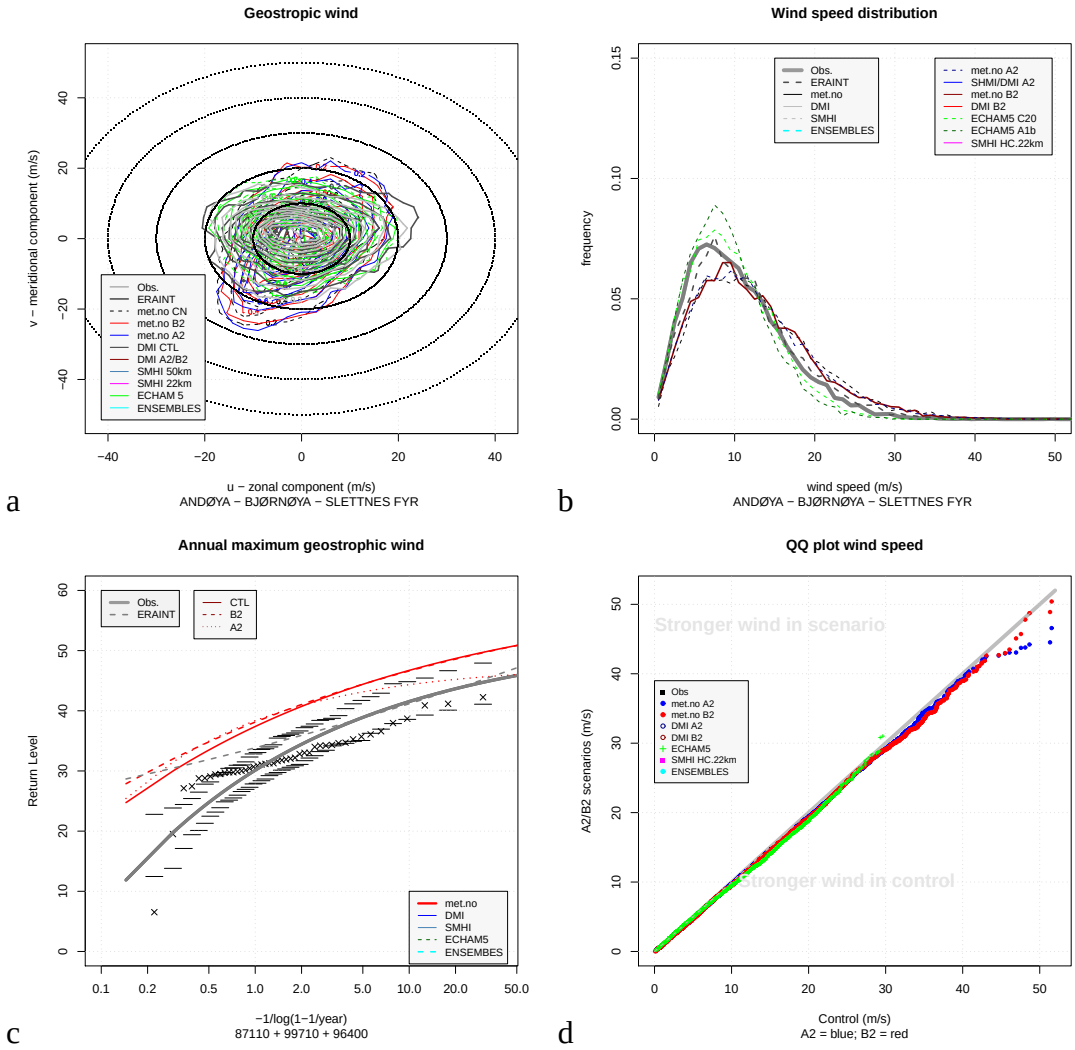

Figure 6: *Same as Figure 4 but for northern Norway, showing a bias in the wind statistics (speed and direction) in the Norwegian HIRHAM results from the PRUDENCE project. Note, the ENSEMBLES results shown here span 1950–2020, the RCMs span 2071–2100, ERAINT spans 1989–2009, while the observations cover the intervals stated in Table* ??

It is also likely that the bias is caused by the rotation of the grid and similar distortions of the SLP near the lateral boundaries of the domain, as seen in Figure 3. However, the distribution curves for the SLP shown in Figure 9 don't suggest severe biases in the SLP, and the shift in the location of these curves are less than for Andøya and Slettnes fyr in Figure 7. It is possible that the stronger geostrophic wind speeds seen in Figure 8 were due to weaker spatial coherence in the Norwegian HIRHAM used in PRUDENCE, or a result of additive effects from biases at all of the three coordinates.

The estimation of winds from triangles (*Alexandersson* et al., 1998, 2000) can only provide some information about winds and storminess. To get a more complete picture, it is necessary to analyse gridded SLP over larger regions. In the next section, we will study low-pressure systems and associated winds through the CCI-analysis and gradient wind equation.

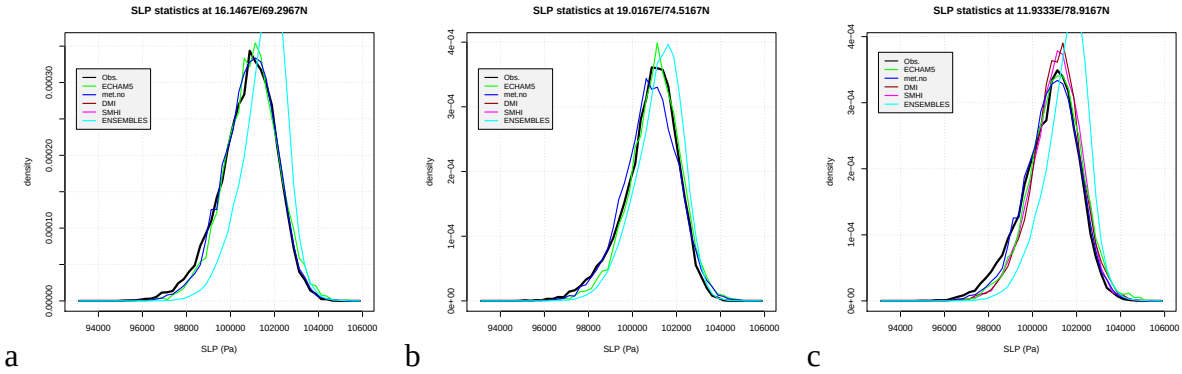

Figure 7: *Same as Figure 5 but for northern Norway. The three panels represent stations 87110 (Andøya), 99710 (Bjørnøya), and 96400 (Slettnes fyr) respectively.*

4.3.1 The 20th century re-analysis

One interesting question is whether there is a good agreement between the 20th century re-analysis and the station observations in terms of geostrophic wind speeds. Figure 10 compares the wind speed estimated from the station observations and the 20th century re-analysis for the three triangles and day-by-day variations. Correlations between geostrophic wind speeds estimated from station observations and the 20th century re-analysis were 0.91, 0.89, and 0.92 respectively. Hence, this comparison suggests a high degree of correspondence between the gridded and station data.

4.4 Storm systems

4.4.1 Storm frequency

Figure 11 shows raw results of the CCI from the ENSEMBLE run with HIRHAM, the positions of local SLP minima and their geographical distribution. The figure shows one map for each decade. It is difficult to tell the difference from such plots, but such differences are more visible in Figure 12 that shows maps of corresponding storm frequencies. While Figure 11 provides more details, Figure 12 represents a gridded analysis where the character of the details are influenced by the grid-box size (10-by-10 degree).

The domain of the RCM limits the distribution of storms in both these figures. The storm frequency, however, is highest over the sea, mainly north of the British Isles and west of Norway.

Figures 13–14 show maps of storm frequency based on the ERAINT data and the 20th century re-analysis respectively. The highest storm frequency is found over the sea and in the vicinity of Iceland and off the east coast of Greenland. There is also a local maxima in the storm frequency near Svalbard. The latitudes greater than 80°N have been masked, due to possible distortion near the latitudinal boundaries and sparse observation network. The reliability of the data in the high Arctic is not known (*Jones*, 1987).

The split between the two maxima near the Bering strait may be an artifact of the analysis, where the longitudinal boundaries may have suppressed the detection of storms.

The 20th century re-analysis storm analysis shown here only covered the north Atlantic region 80°W–40°E and 20°N–75°N. The local maximum in storm frequency from the 20th century re-analysis is consistent with the CCI-analysis based on the ERAINT data. The different

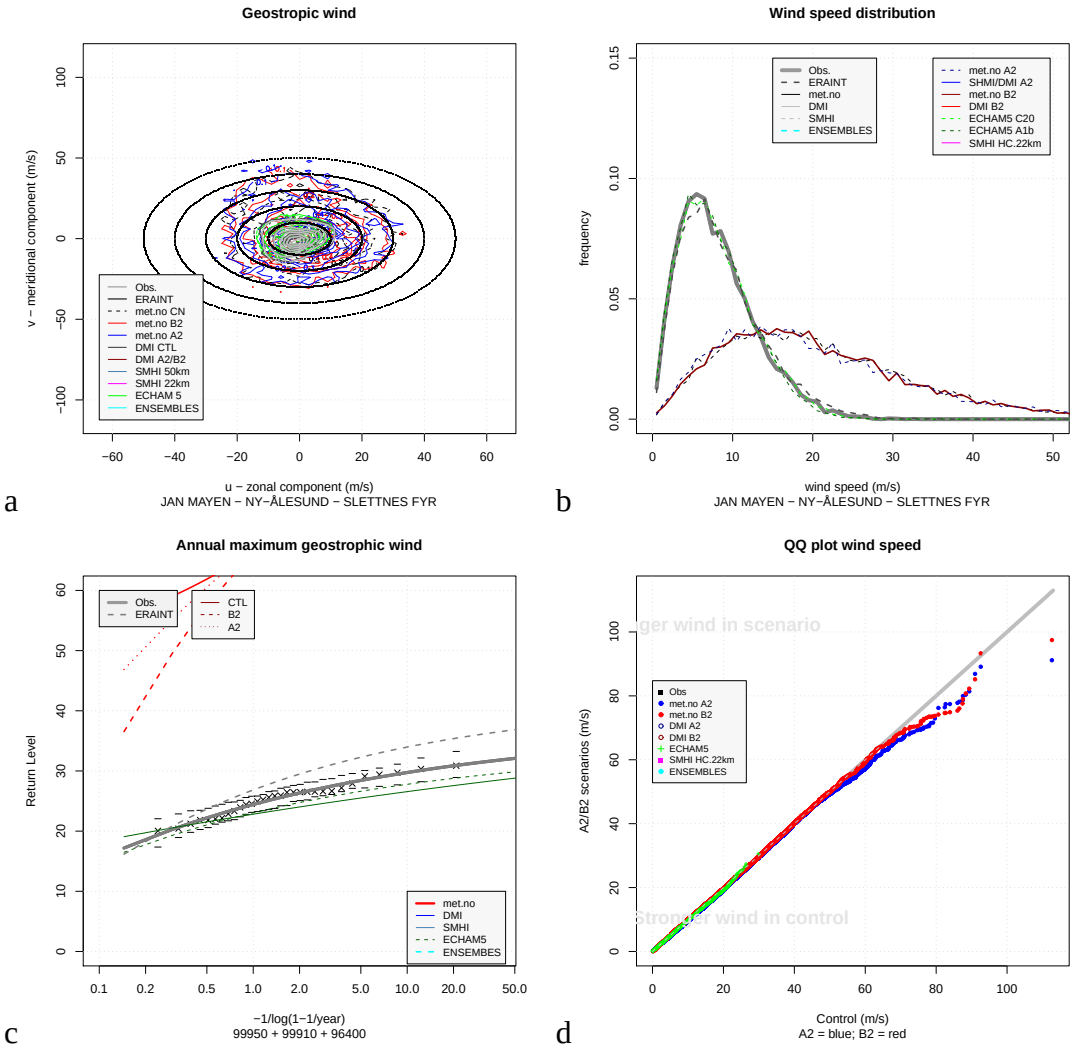

Figure 8: *Same as Figure 4 but for the Arctic region, showing a bias in the wind statistics (speed and direction) in the RCAO and Norwegian HIRHAM results from the PRUDENCE project. Note, the ENSEMBLES results shown here span 1950–2020, the RCMs span 2071–2100, ERAINT spans 1989–2009, while the observations cover the intervals stated in Table* **??**

30-year intervals differ only in detail (e.g. numbers due to incomplete 30-year intervals at the beginning and end of this analysis period), but the main features seem to be robust.

Figure 15 compares some storm statistics from the ERAINT and the HIRHAM ENSEMBLES simulation over the region corresponding to the RCM domain. The statistical distribution of the SLP central pressure is somewhat biased to higher values in the RCM (panel a), and hence the RCM has a tendency to underestimate the depth of these cyclones. Nevertheless, the RCM yields higher gradient wind speed estimates (panel b), and the storm systems in the RCM results tend to be smaller than the in CCI storm statistics derived from the ERAINT data (panel c). These observations appear to be consistent with equation 3, in which the gradient wind speed increases with smaller storm radius. Panel d shows the relationship between the gradient wind speed and latitude, and the RCM produces greater values for all latitudes. For both RCM and ERAINT, the wind speed estimates appear to be fairly uniformly distributed with latitude.

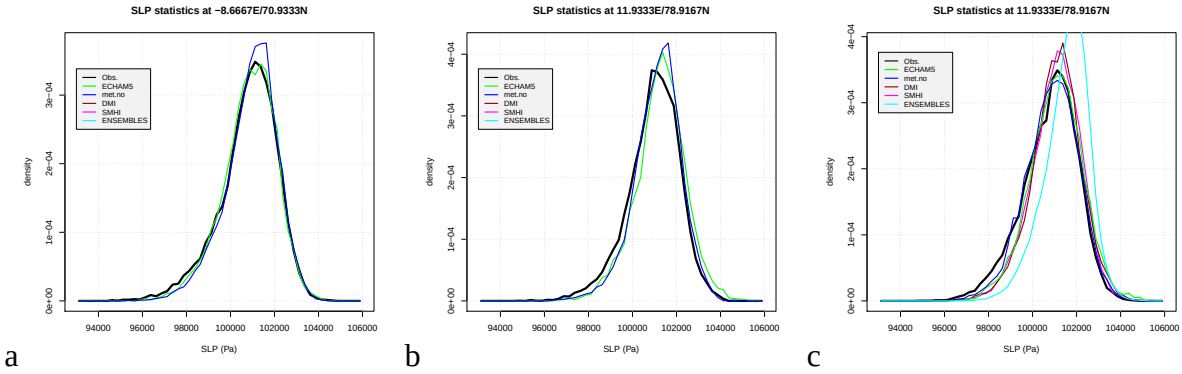

Figure 9: *Same as Figure 5 but for the Arctic region. The three panels represent stations 99950 (Jan Mayen), 99910 (Ny Ålesund), and 96400 (Slettnes fyr) respectively.*

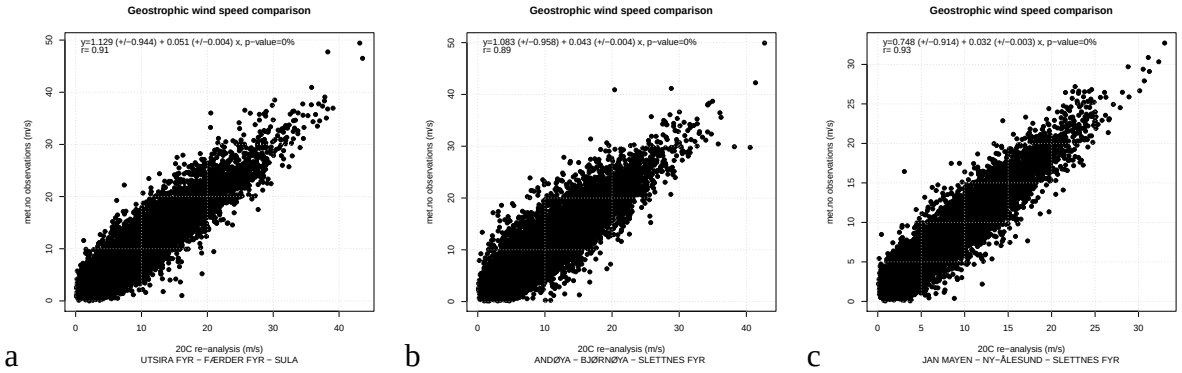

Figure 10: *Scatter plot of geostrophic wind speed estimates from triangulation of the 20th century re-analysis and station observations. These analysis provide a comparison between black symbols and grey curves in Figures 21–23.*

Figure 16 shows a similar analysis as Figure 15, but for the 20th century re-analysis and ERAINT, rather than ERAINT-RCM. The statistical distribution of the 20th century re-analysis (black curve in panel a) exhibits a peak at the same central pressure as the ERAINT (blue), and both show similar distribution curves for the gradient wind estimates. The storm radius estimates show some variations in the statistics at the small end, but the curves converge at scales greater than 200km. A curious feature is that both show tendencies with peaks at $\sim$300km and $\sim$400km.

The 20th century re-analysis also shows a tendency of stronger winds at higher latitudes. There are some stronger wind events in the 20th century re-analysis, but not enough to seriously affect the distribution in panel b. A longer interval, as represented by the 20th century re-analysis, is expected to be associated with more extreme events.

4.4.2 Time evolution of wind and storminess

Time series showing how the storm statistics change from year to year and over longer times are interesting in many aspects, but it is important to keep in mind that reanalysis products such as ERAINT and the 20th century re-analysis involve observations from a network that has changed over time (*Bengtsson* et al., 2004). Nevertheless, the trend analysis based on these reanalysis

products represent our best knowledge about long-term changes in the statistics of past weather events.

Figure 17 shows the time evolution of the annual gradient wind speed statistics (upper) and the annual storm count (lower) for both the HIRHAM ENSEMBLES run and ERAINT. In other words, the upper panel gives an indication of how the storms intensity has varied over time whereas the lower panel shows how the frequency has changed. Again, higher extreme wind estimates in the RCM results are evident. There is better agreement between the RCM and ERAINT on the quantiles, however. Neither RCM nor ERAINT suggest there is any pronounced long-term trend in either gradient wind speed or storm frequency over the region corresponding to the RCM domain.

Figure 18 shows a similar analysis as in Figure 17, but this figure shows a comparison between the 20th century re-analysis and ERAINT rather than between ERAINT and the RCM. Thus this figure provides a picture of the long-term evolution of the annual gradient wind speed statistics and the annual storm count. The CCI-analysis based on 20th century re-analysis and ERAINT suggest similar values, albeit with some differences in the details; The 20th century re-analysis suggests slightly greater maximum wind speeds. There is no pronounced trend in the evolution of these storm statistics in the region corresponding to the RCM domain. A linear trend fit, however, nevertheless hints at a positive trend in the number of storms that have a central SLP deeper than 960hPa, as the slope of the line number against year is 0.0067 ± 0.0039 ($\pm$standard error), with a p-value of 9%. Thus, the data suggest that there has been only modest - if any - changes in the storm statistics over time and over the limited region in question.

Figure 18 only gives a picture of the storm statistics over a limited region of the north-Atlantic. The same analysis for 80°W–40°E and 20°N–75°N (Figure 19) suggest more pronounced trends in the storm statistics over time. Furthermore, the maximum wind-speed estimates derived from the 20th century re-analysis are slightly greater than for the limited region surrounding the Nordic countries; even exceeding 100 m/s.

The regression of the maximum wind speed against the calendar year has a slope with -0.17 ± 0.06 and a p-value of 0.005 (upper panel). Hence this trend analysis suggests that the trend is statistically significant at the 1%-level. It is important to ask whether this change is for real, or due to non-homogeneities (*Bengtsson* et al., 2004). If real, then the interesting question is why the maximum wind speeds have varied, why they are lower now, and what are the causes.

The linear regression of the counts of storms with central SLP lower than 960hPa against the year also has a slope of $+0.06 \pm 0.015$ (lower panel), and is associated with a p-value of 9.74×10^{-5}; hence statistically significant at the 1%. Again, caution is needed when looking at trends in re-analysis products, as changes in the observing system may introduce non-homogeneities (*Bengtsson* et al., 2004). Nevertheless, the trend analysis for the larger region contrasts the same analysis for the limited region in Figure 18. Thus, a smaller region may give different impression about trends in storminess than a larger region.

One impression from Figure 19, however, is a more steady state since the 1940s, and that the trends are affected by the difference between the early part when the annual maximum wind estimates exhibit more pronounced fluctuations and the later part.

Figure 20 presents a number of statistics of the storms in the region 80°W–40°E and 20°N–75°N for the 20th century re-analysis. As with Figure 16 for the RCM domain, the statistical distributions of the central SLP and gradient wind speed seem to be roughly consistent in the ERAINT and 20th century re-analysis (no Kolmogorov-Smirnov test has been performed,

though). These two analyses differ in the latitudinal distribution of the gradient wind speed: the 20th century re-analysis indicates greatest values at high or low latitudes with a minimum near 50°N.

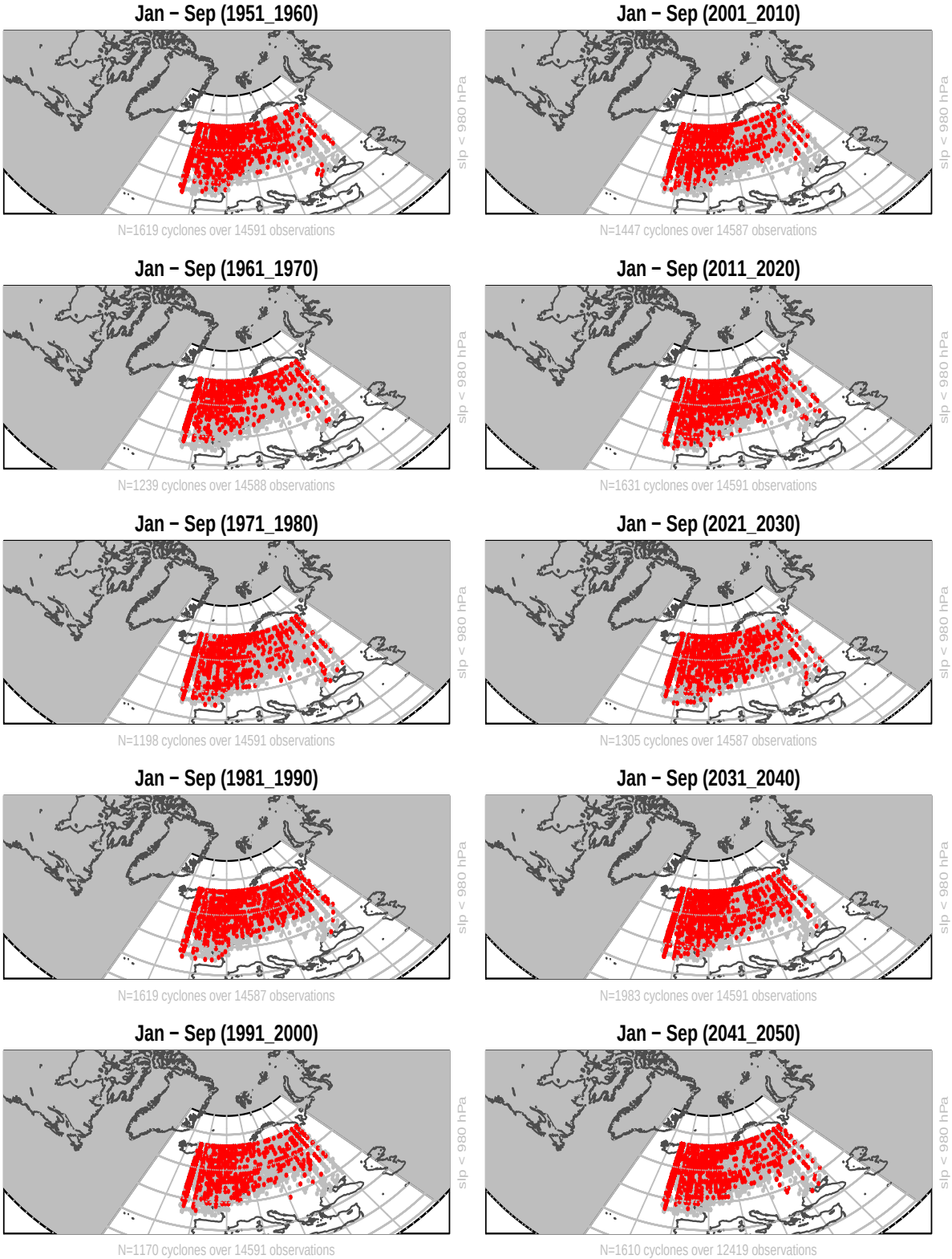

Figure 11: *The location of cyclones according to CCI. The grey symbols mark the locations of all cyclones whereas red only represent the locations for the a given decade. Only systems with central pressure below 980hPa have been counted.*

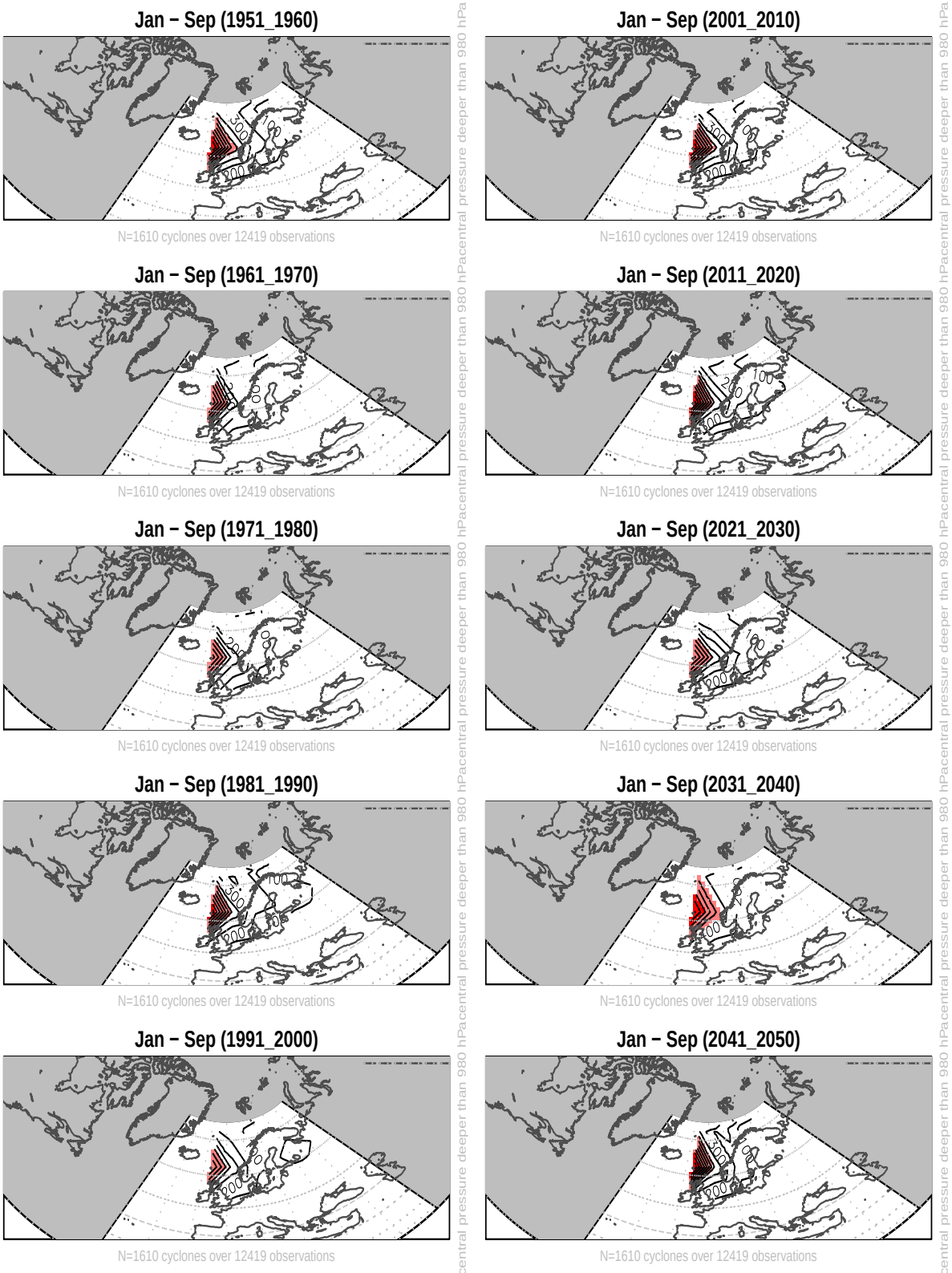

Figure 12: *The density of cyclone counts - also referred to as 'storm frequency'. Most of the storms are seen in maritime regions near the British isles in the Norwegian HIRHAM from the CES. Furthermore, the RCM domain is too small for providing a detailed picture. Only systems with central pressure below 980hPa have been counted.*

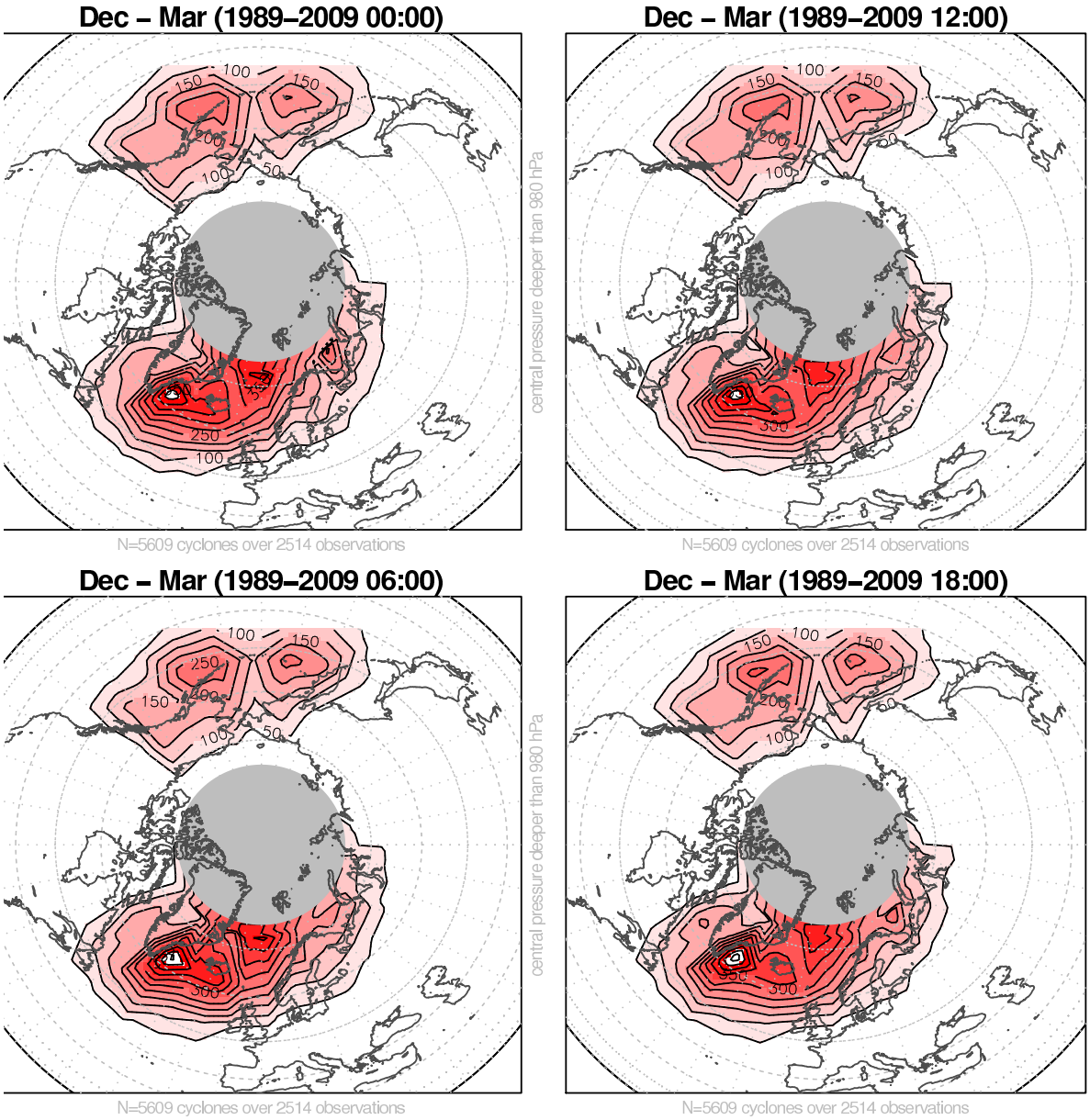

Figure 13: *Storm frequency (counts) based on the ERAINT. The different panels show storm frequencies for different times in the day: 00:00, 06:00, 12:00, and 18:00. The similarity between the results at different times of the day suggest that the detection analysis is reasonably robust, as it the storm occurrence is not expected to be sensitive to the time of the day.*

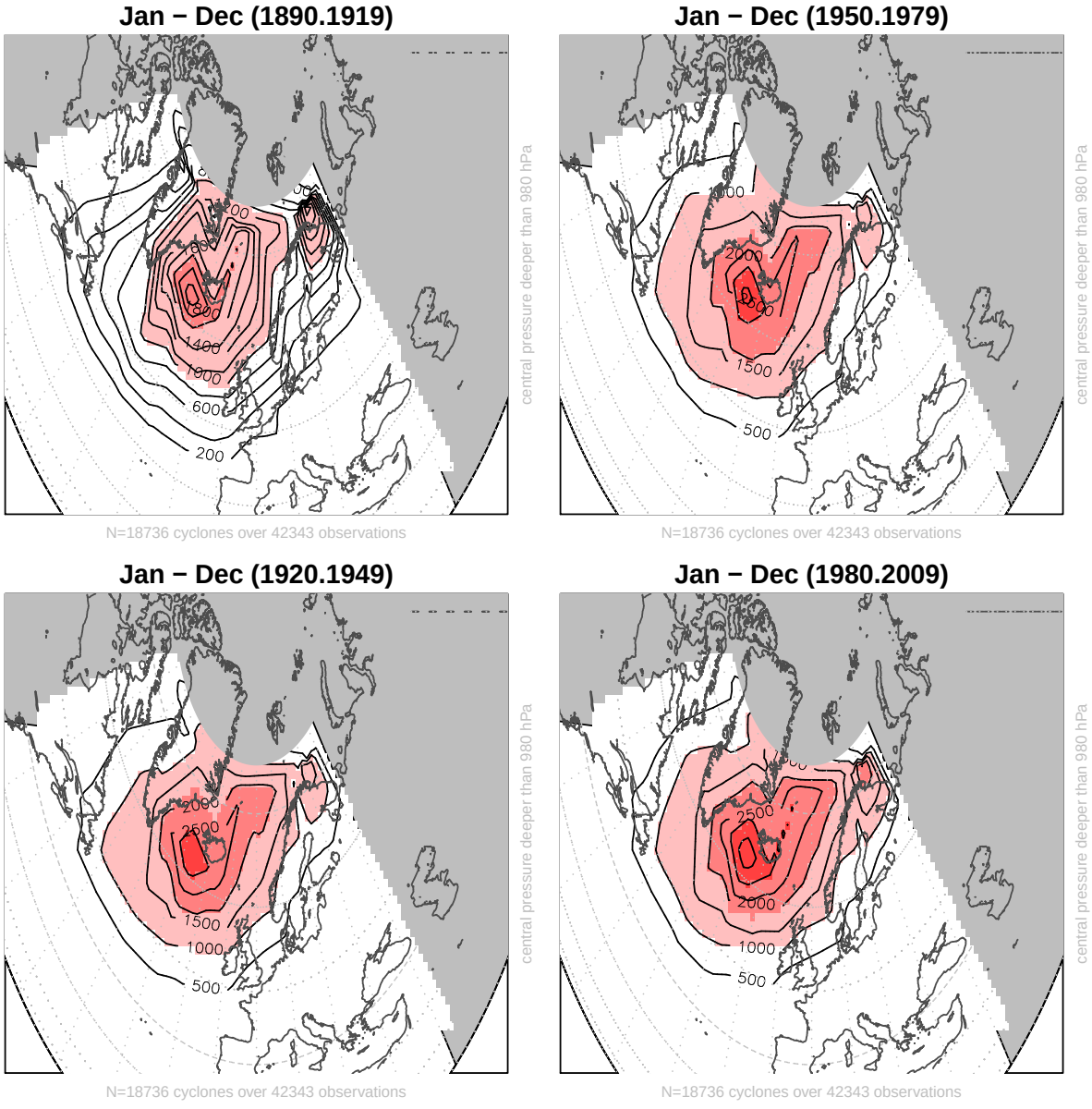

Figure 14: *Storm frequency (counts) based on the 20th century re-analysis. Here the panels show maps for different 30-year periods: 1890–1919 (the actual data starts in 1891, however), 1920–1949, 1950–1979, and 1980–2009 (the analysis stops December 31st, 2008).*

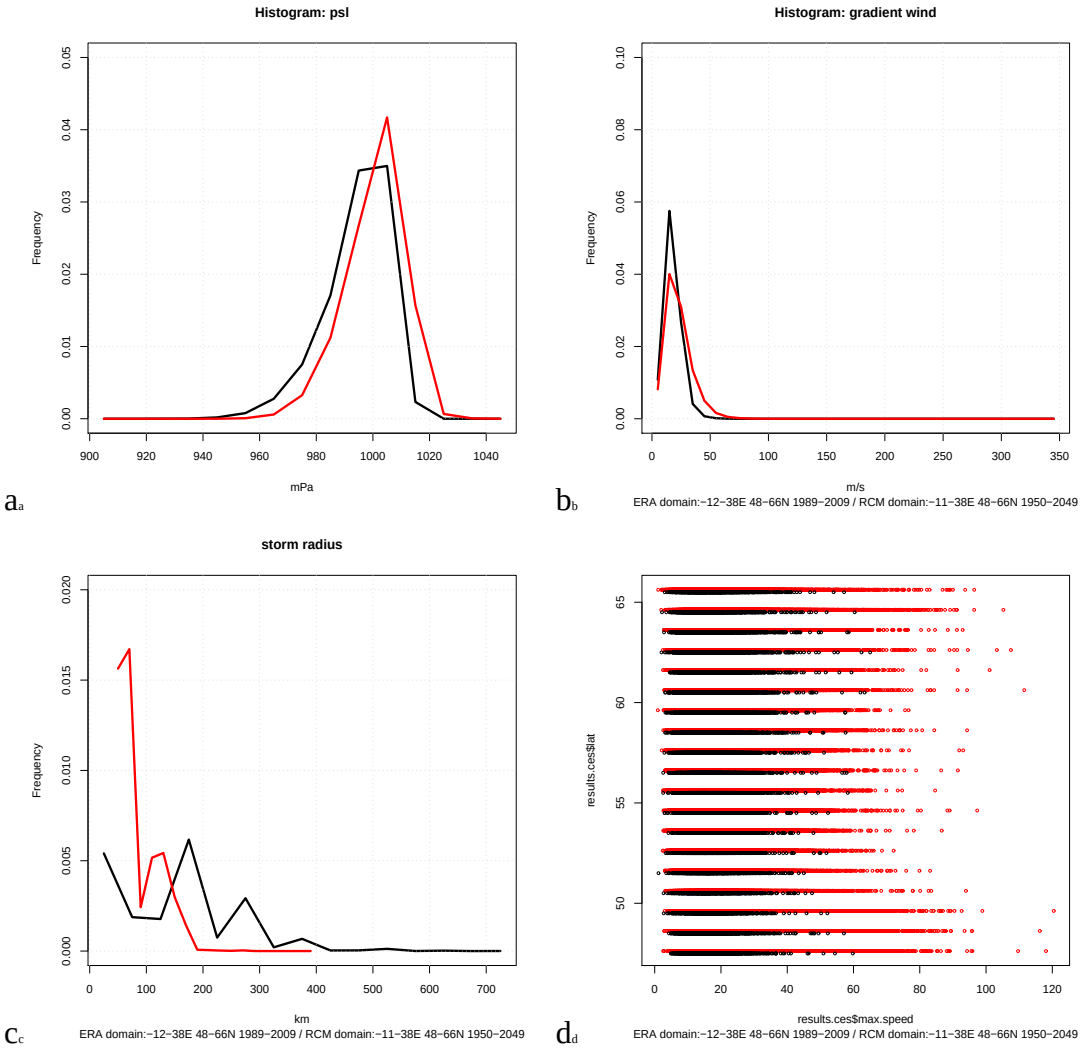

Figure 15: *Summary of some storm statistics: the statistical distribution of the central sea-level pressure, gradient wind speed, storm radius, and the relationship between gradient wind speed and latitude. Black curves represent the ERAINT re-analysis while red show results from the HIRHAM ENSEMBLES simulation.*

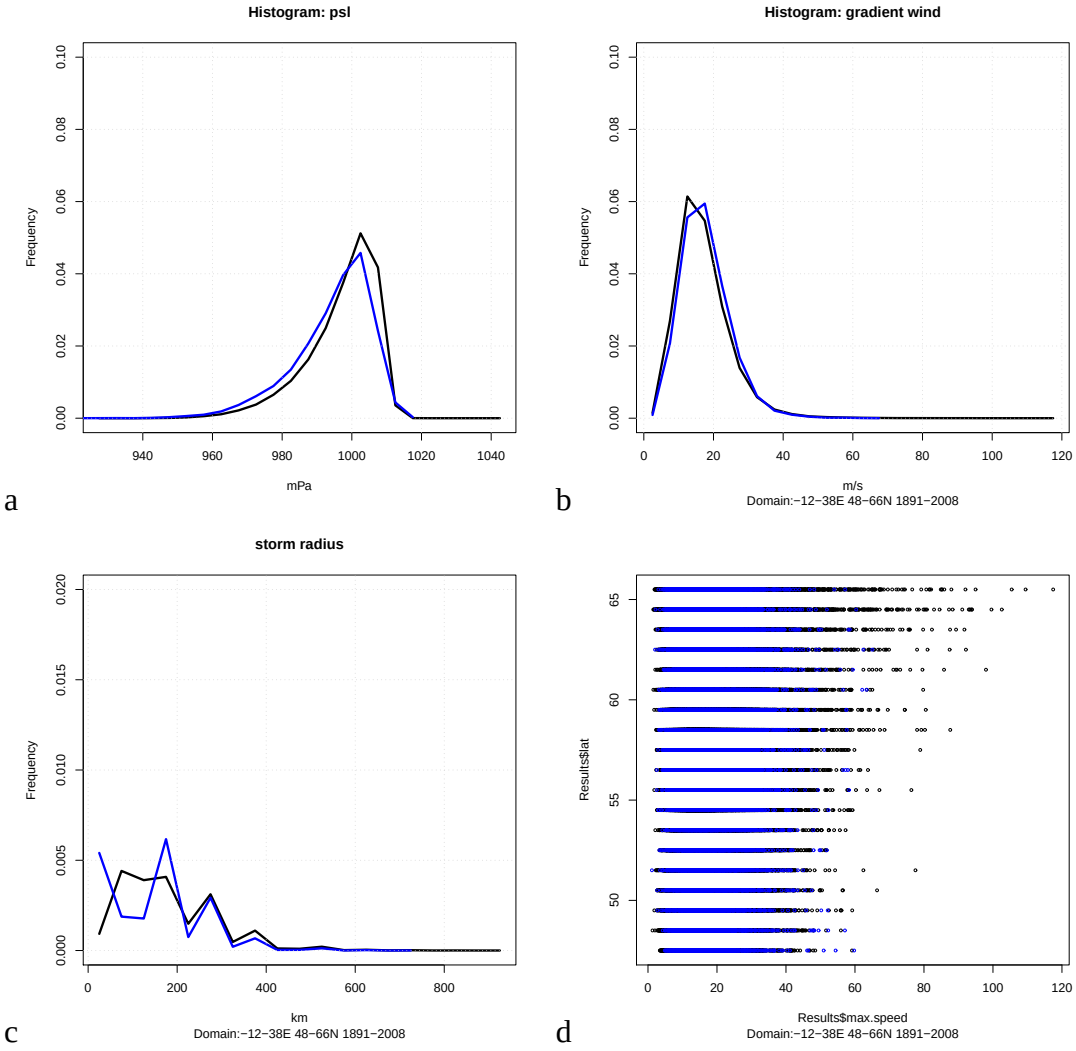

Figure 16: *Similar statistics as shown in Figure 15, but here the storm statistics is between ERAINT (blue) and the 20th century re-analysis (black).*

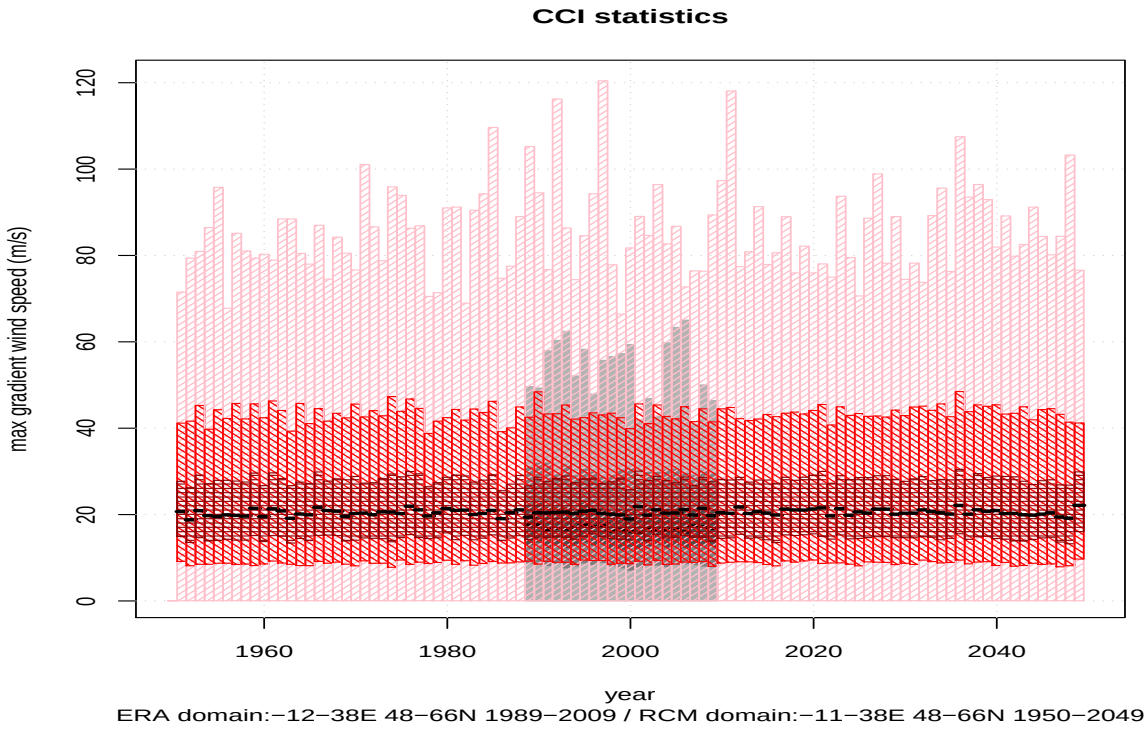

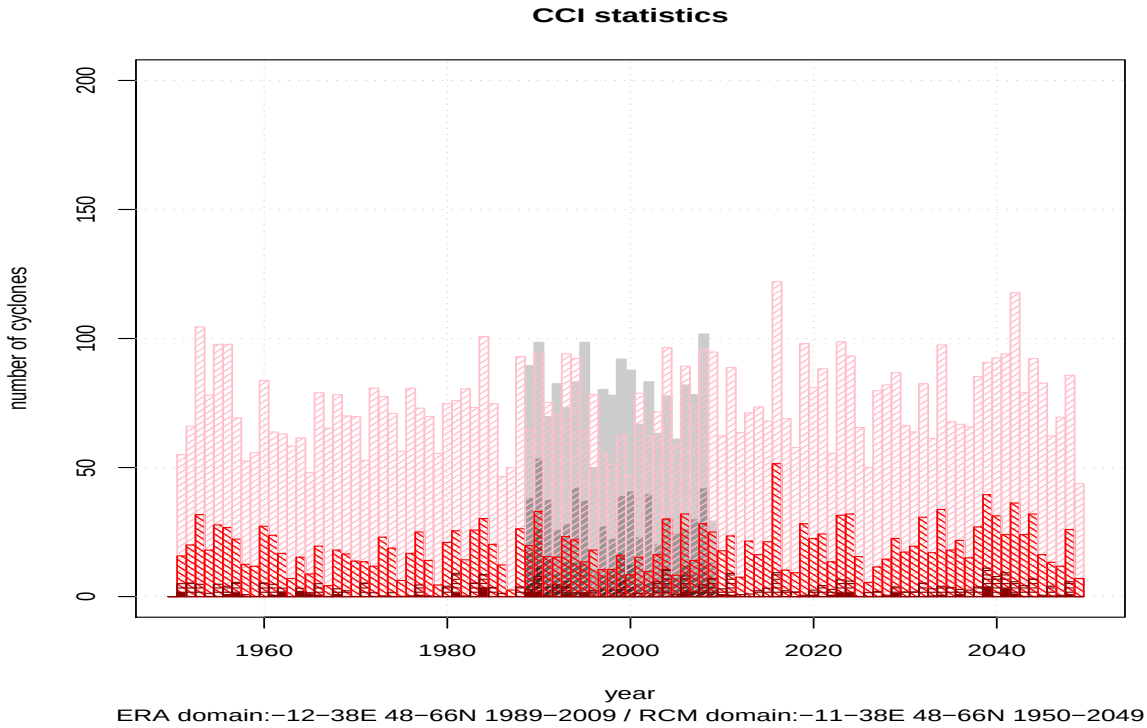

Figure 17: *The time evolution of the annual statistics of the gradient wind speed (upper) and the storm counts (lower) based on the HIRHAM ENSEMBLES simulation (red) and ERAINT re-analysis (grey). The different colours and hatching in the upper panel mark the annual maximum value, the 95-percentile, 75-percentile, 25-percentile and the 5-percentile each year. In the lower panel, the different levels shown by colour and hatching mark threshold values of 990hPa, 980hPa, 970hPa and 960hPa.*

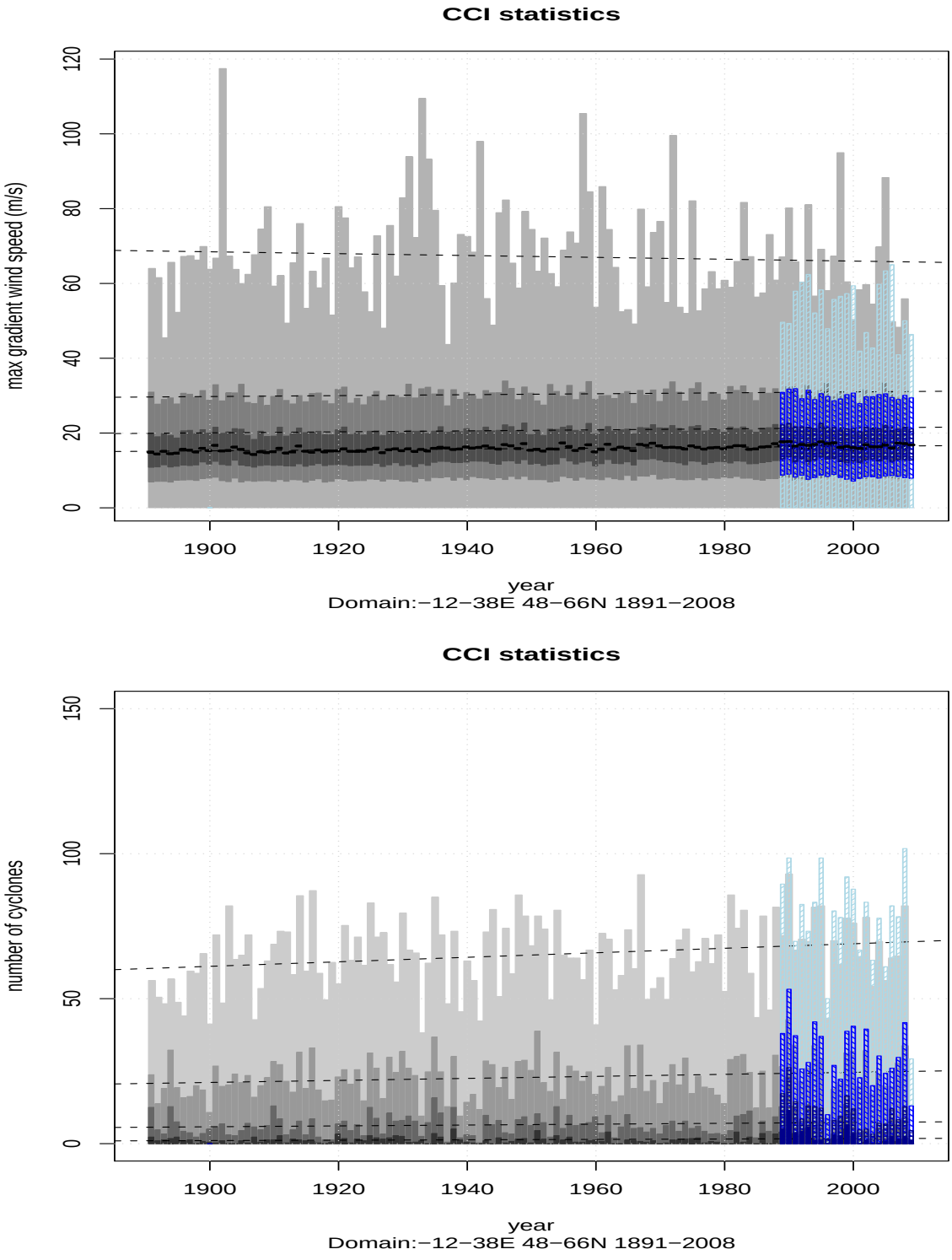

Figure 18: *Similar analysis as in Figure 17, but for the ERAINT (blue) and the 20th century re-analysis (grey). The storm statistics are summarised for the same region as covered by the HIRHAM ENSEMBLES domain. The dashed lines in the figure mark the results from a regression of the wind-speed quantiles or storm counts against time.*

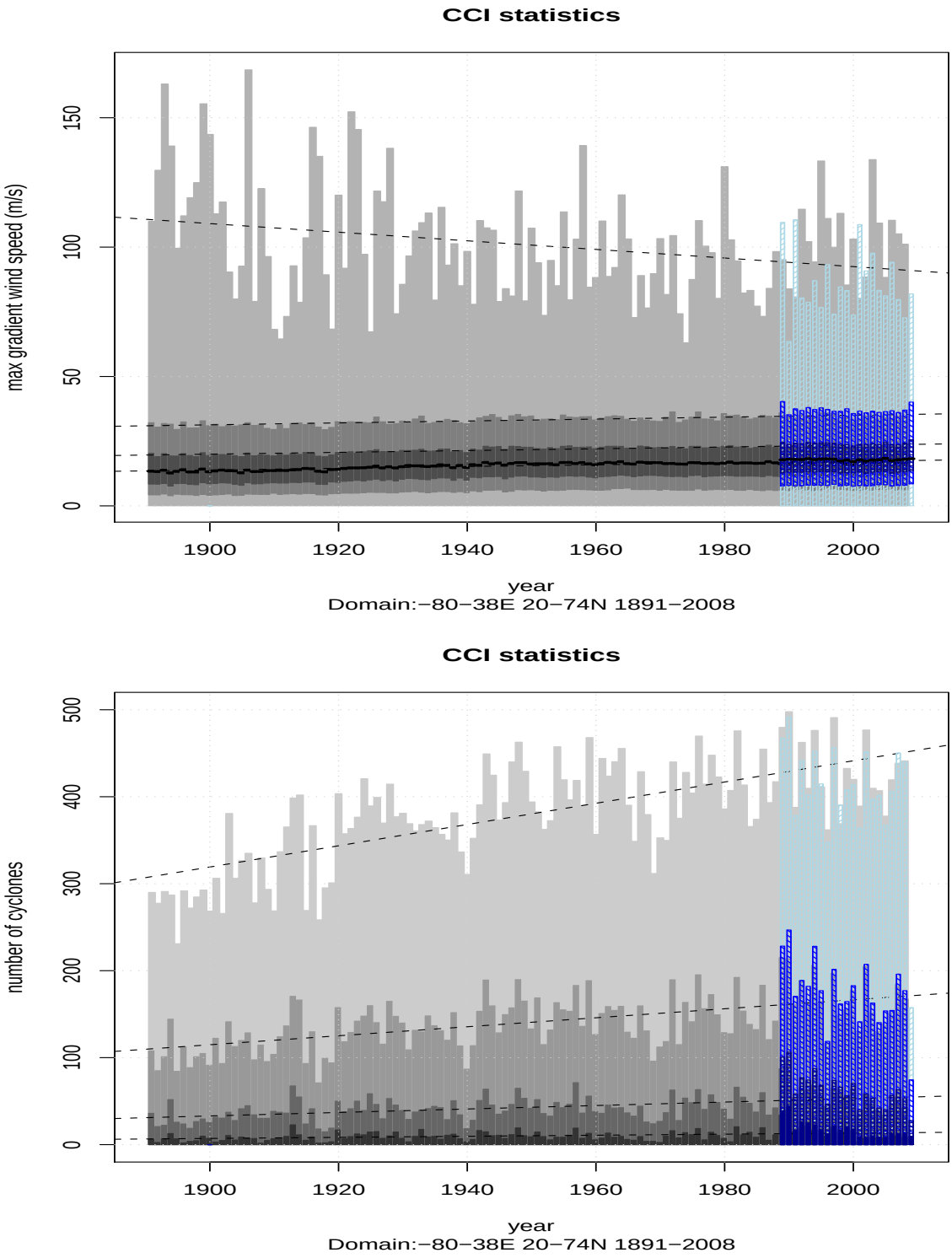

Figure 19: *Same as Figure 18, but for a larger region covering most of the north Atlantic.*

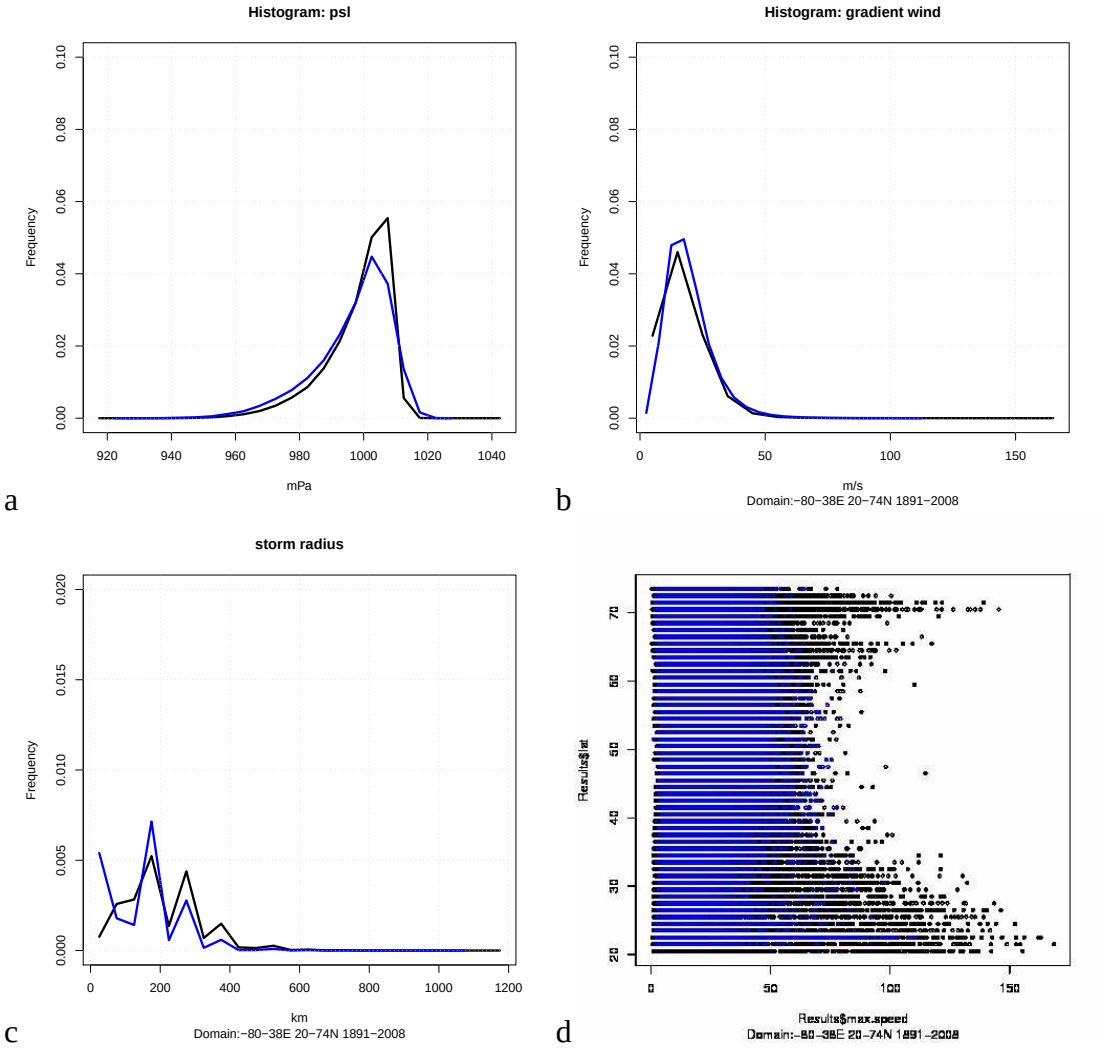

Figure 20: *Same as Figure 16, but for a larger region covering most of the north Atlantic. ERAINT is shown in blue and the 20th century re-analysis in black.*

4.4.3 Time evolution of wind estimates

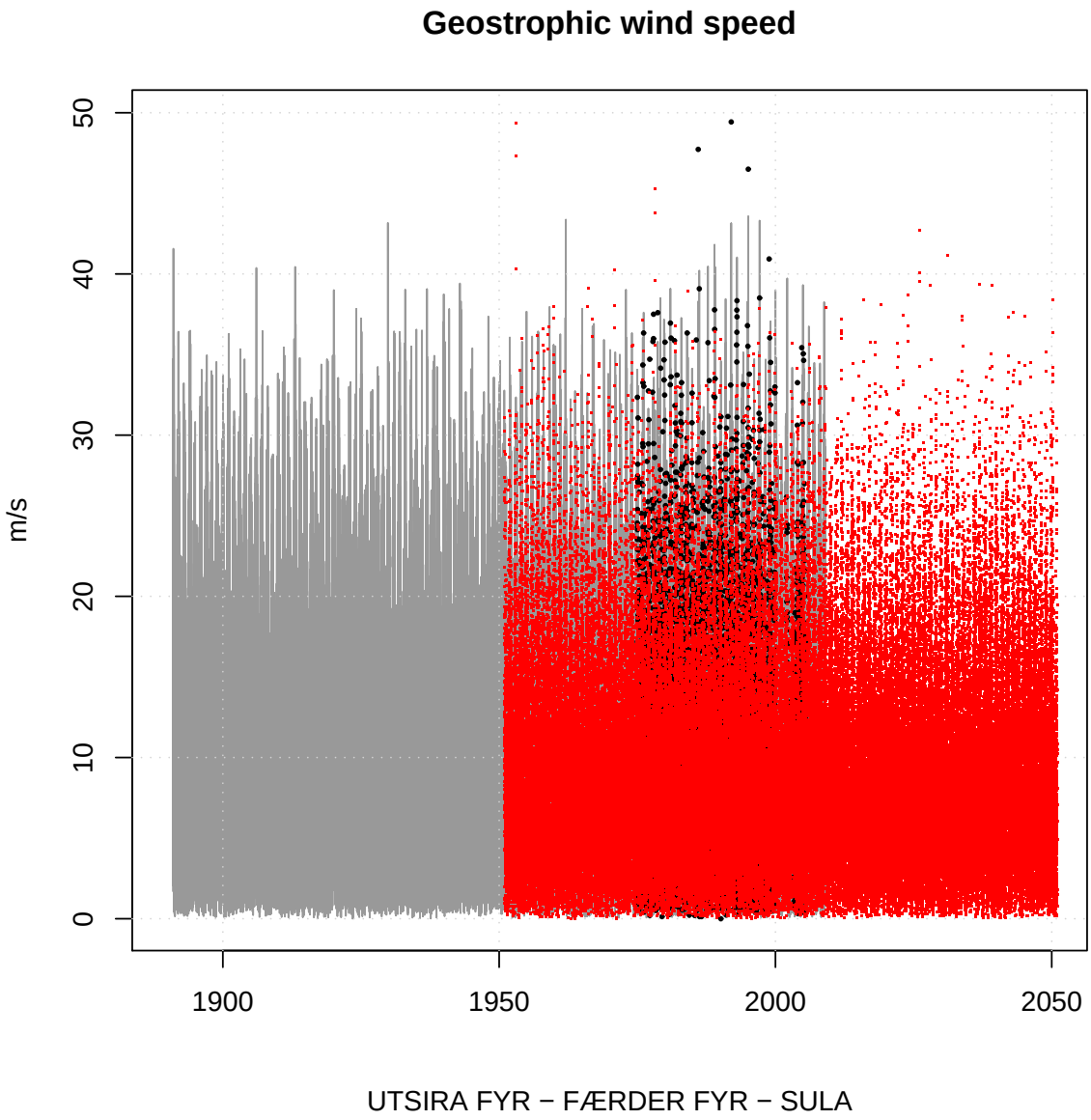

Figure 21: *Geostrophic wind speed estimates from triangulation, based on the 20th century re-analysis (grey), station observations (black) and the RCM ENSEMBLES run (red).*

Figures 21–23 show time series of the wind estimates from triangulation for southern Norway, northern Norway, and the Arctic (Figure 2). Note, the triangles for northern Norway and the Arctic region were outside the RCM domain. There is a reasonable agreement in magnitude between all these results, and there is no clear unambiguous trend in the estimates.

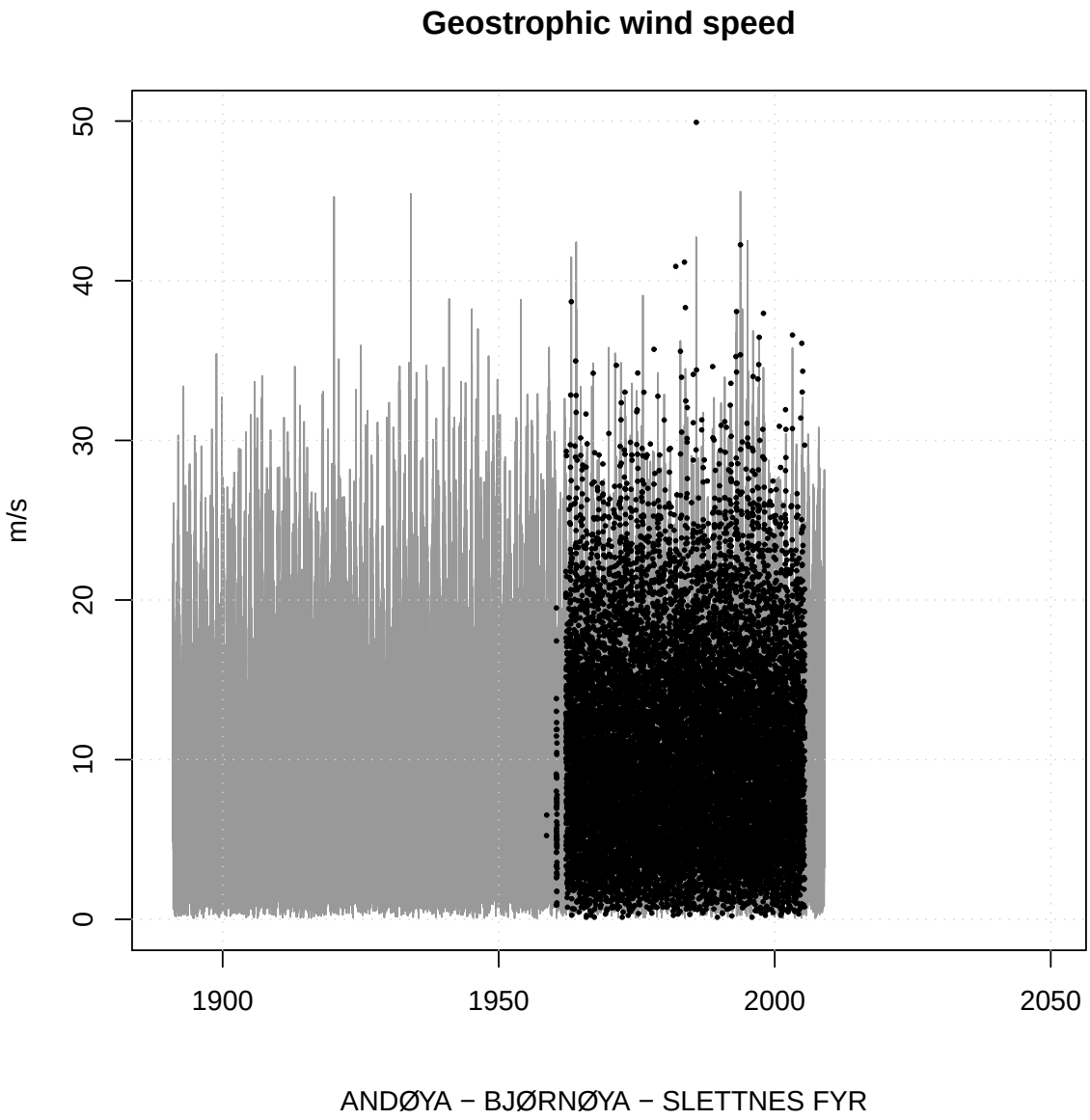

Figure 22: *Geostrophic wind speed estimates from triangulation, based on the 20th century re-analysis (grey) and station observations (black).*

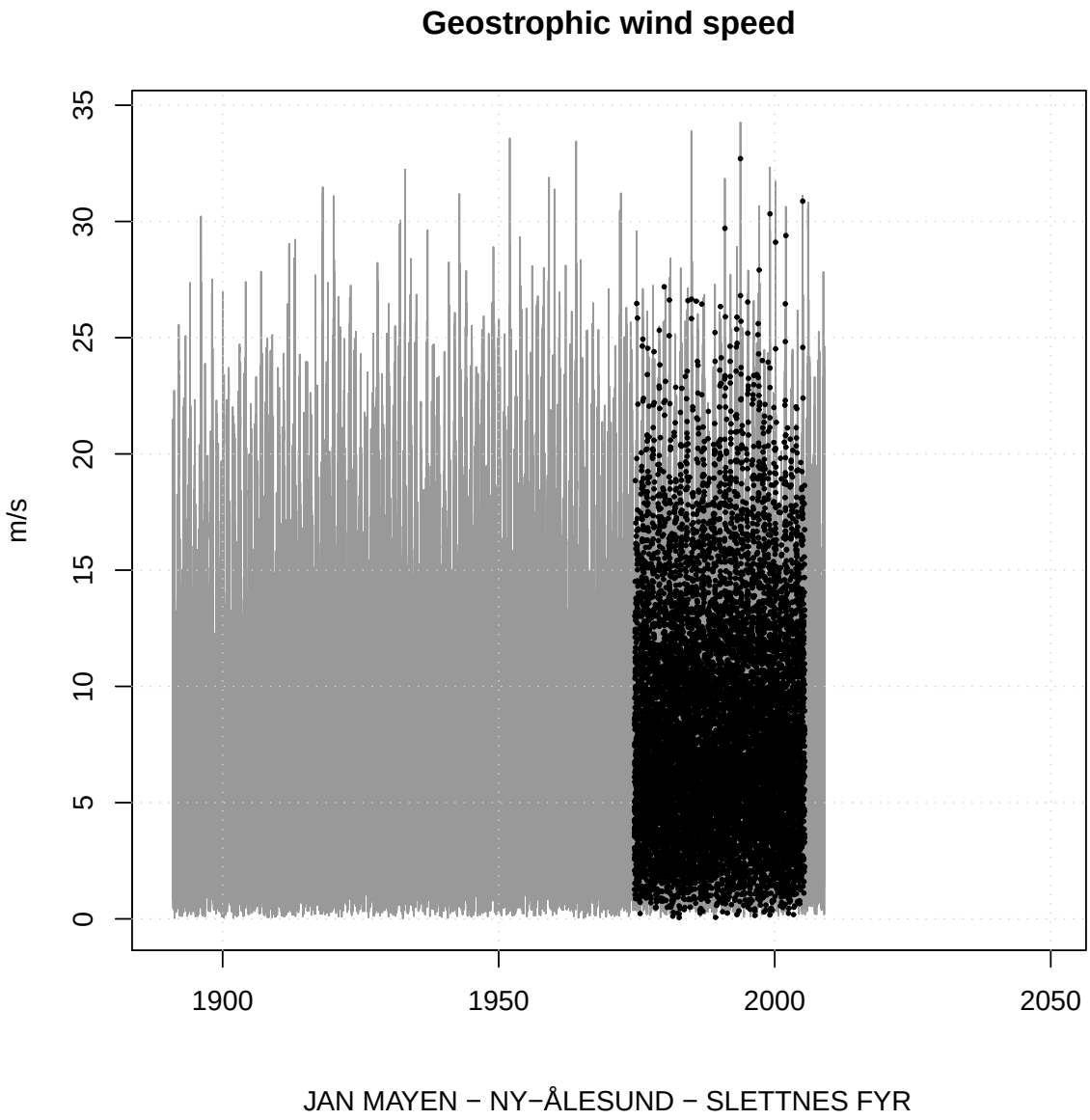

Figure 23: *Geostrophic wind speed estimates from triangulation, based on the 20th century re-analysis (grey) and station observations (black).*

5 Discussion

An interesting question is why there is a pronounced maximum in storm frequency between Iceland and Greenland. It is known, however, that storm cyclogenesis is affected by the position of the jet stream, geography, availability of heat, and temperature gradients. Another interesting question is whether the North-Atlantic Oscillation (NAO) is a manifestation of the storms, or whether the storminess is a result of the NAO and is driven by large-scale SLP anomalies.

The RCMs presented here have been driven with only a small set of GCMs (ECHAM4 & HadAM3H, Table 2), and they were therefore not entirely independent. In fact, one would expect the SLP in the different RCMs to be similar if their domain is small and the solutions dominated by the GCM fields. On the other hand, the RCM-based (driven by HadAM3H) winds in Figure 8 were substantially different to those derived from the GCM (ECHAM5). This difference may be due to using different GCMs for driving the RCMs, and the fact that HadAM3H is an AGCM for which observed SST and sea ice were prescribed (together with a projected change), whereas ECHAM4 represented a fully coupled AOGCM (Erik Kjellström, private communication). If sea surface temperatures (SSTs) and sea-ice were prescribed differently at high latitudes for the different GCMs, this could also affect the storm statistics (*Benestad* et al., 2010).

One concern is that the RCM domain really is too small to represent well the statistics of storms with a spatial extent of 100–300 km. The triangulation may also be affected if some of the station locations (nodes of the triangle) were in the vicintiy of lateral borders of the RCM domains because of distortions near the lateral boundaries (Figure 3).

One caveat with storm statistics derived from global climate models (GCMs), regional climate models (RCMs), and re-analysis is that the role of clouds in the growth of instability may not have fully been captured. Although numerical models have demonstrated that large-scale dynamics alone can reproduce the instabilities necessary to generate low-pressure systems such as mid-latitude cyclones, thermodynamics may also play a role. Buoyancy and air flow may be affected by condensation on small unresolved spatial scales.

Another question is whether the 20th century re-analysis is homogeneous (*Bengtsson* et al., 2004). On the one hand, barometers are considered to be fairly reliable and have not changed much over time, and the coverage over the sea has never been very dense. The density of the near-surface measurements in the north-Atlantic - where the storm frequency is highest - has diminished since the 1940s as the number of weather ships has dropped to one in 2008 (zero in 2010). The number of locations where the near-surface temperature and sea surface temperature (SST) have been measured, however, increased over the first part of the 20th century.

One question is whether wind speeds exceeding 100m/s are realistic. A category 5 hurricane on the Saffir-Simpson scale[3] has wind-speeds greater than 70 m/s, and values greater than the speed of sound (343 m/s in dry air at 20°C) are not credible. However, the gradient and geostrophic wind estimation represent the free atmospheric flow, rather than surface winds used to categorise hurricanes. The air flow near the surface is subject to friction and thus upper air winds may involve higher speeds. The wind-estimation and the geostrophic equation also breaks down at low latitudes where $f(\phi) \rightarrow 0$. Hence, the lower latitude of the region of analysis was cut-off at 20°N, but the highest estimates for wind speed in both ERAINT and 20th century re-analysis were found at the low latitudes (Figure 20). The 20th century re-analysis also

[3] http://en.wikipedia.org/wiki/SaffirSimpson_Hurricane_Scale

indicated extreme values near 70°N, not seen in ERAINT. The triangulation analysis suggest maximum geostrophic wind speeds in the interval 40–50 m/s for HIRHAM (ENSEMBLES) (Figure 21), but this magnitude was also reasonably consistent with the geostrophic wind analysis for ERAINT and the station measurements. Panel c in Figures 15 and 16 shows the gradient wind speed estimates from the CCI-analysis, with values for maximum winds at latitudes near 60°N in the interval 40–60 m/s for ERAINT/20th century re-analysis and $\gtrsim$100m/s for HIRHAM.

There is an interesting observation: there is little trend in the small region similar to the domain of the RCM, but there were more pronounced trends if we look at the whole basin. The lack of clear trend in storminess around Norway is consistent with previous analysis for 1961–2006 based on direct wind measurements from four coastal wind meters, carried out by Knut Harstveit (*Hanssen-Bauer* et al., 2009, Figur 3.1.10), where the wind speeds exceeding $21m/s$ were taken as a storm event. The differences in trends for the storm statistics also suggests that they represent a regional feature, with different trends in different regions, as shown in *Benestad & Chen* (2006). Hence, a study based on a limited region may not capture important aspects. Furthermore, this leads to the question of whether it is best to use a large RCM domain rather than a small RCM domain. For small domains, the SLP is to a greater extent determined by the driving GCM. Thus the storm statistics will to a greater degree depend on the GCM and resolution. The detectability of storm systems may be sensitive to resolution (*Blender & Schubert*, 2000). A larger RCM domain may capture more events by covering a greater region in addition to being less constrained by the SLP from the GCM. Thus providing a greater region with high resolution where storms can develop may possibly affect the simulation of the storm statistics, especially if the storms upscale and affect the ambient environment through horizontal and vertical heat, momentum, and mass transport. Storms that would form outside the region of a small domain, if sufficiently high spatial resolution, may potentially not materialise in a simulation with a small RCM domain. Furthermore, is is not clear whether the trajectory of the storms were affected by the spatial resolution. However, RCMs with large domains may simulate large-scale dynamic solutions that are inconsistent with the GCM results. Techniques such as 'spectral nudging', however, can be introduced to alleviate such inconsistencies (*von Storch* et al., 2000). It is also evident from Figure 17 that the number of storms in the RCM match the number of storms in ERAINT fairly well, albeit with a slight low bias..

The main conclusion from *Wern & Bärring* (2009) was that the greatest wind speeds increased in 5 but decreased in 6 triangles over Sweden (11 triangles in total), and that there was no statistically significant trend over the country as a whole. They also found that number of events with wind speeds exceeding 25 m/s had been reduced in 7 of 11 of the triangles, and that the mean wind speed had diminished in 10 of 11 since 1951. The findings of *Wern & Bärring* (2009) are consistent with independent analyses presented here.

6 Conclusion

An analysis of storm systems based on mean sea level pressure, geostrophic wind estimation, gradient wind analysis, and calculus-based cyclone identification suggests that there are differences between the results from regional climate models and observations. The regional climate models predict different storm system wind speeds than derived from observations. The validity of these analyses are expected to be limited by the accuracy of the re-analysis, however,

although the results in general appear to be realistic. By and large, the storm statistics derived from the 20th century reanalysis for 1891–2008 and the more recent ERAINT for 1989–2009 show consistent statistics. The analysis also suggests that RCMs with small domains may miss interesting features elsewhere in the north-Atlantic.

In conclusion, the analysis don't give clear indications of long-term changes in the storm statistics over the North Atlantic for the future, and there are uncertainties due to the spatial coverage associated with observational network of the past that place a limit to the confidence that can be given the trend-analyses for the 20th century, as the number and density of maritime barometric measurements over the North Atlantic have changed over time.

Acknowledgements

This work has been supported by the Norwegian Meteorological Institute. Jan Erik Haugen kindly provided the HIRHAM RCM data. The analysis of the storm statistics from the HIRHAM RCM was done for the 'Climate and Energy Systems' (CES) project[4], whereas the storm statistics derived from the ERA Interim was done under SPAR[5] (IMILAST[6]). Torill Engen-Skaugen and Erik Kjellström have given valuable feedback and comments on this manuscript. Support for the Twentieth Century Reanalysis Project dataset is provided by the U.S. Department of Energy, Office of Science Innovative and Novel Computational Impact on Theory and Experiment (DOE INCITE) program, and Office of Biological and Environmental Research (BER), and by the National Oceanic and Atmospheric Administration Climate Program Office.

[4]http://en.vedur.is/ces

[5]http://projects.met.no/spar/

[6]http://www.proclim.ch/IMILAST/index.html

References

Alexandersson, H., Schmith, T., Iden, K., & Tuomenvirta, H., 1998. Long-term variations of the storm climate over NW Europe. *The Global Atmosphere and Ocean System*, **6**, 97–120.

Alexandersson, H., Tuomenvirta, H., Schmith, T., & Iden, K., 2000. Trends of Storms in NW Europe derived from an updated pressure data set. *Climate Research*, **14**(1), 7173.

Benestad, R.E., & Chen, D., 2006. The use of a Calculus-based Cyclone Identification method for generating storm statistics. *Tellus A*, **58A**(doi:10.1111/j.1600-0870.2006.00191.x), 473–486.

Benestad, R.E., Senan, R., Balmaseda, M., Melsom, A., & Ferranti, L., 2010. Predictability on seasonal scales associated with sea ice. *submitted to Tellus A*.

Bengtsson, L., Hodges, K.I., & Hagemann, S., 2004. Sensitivity of the ERA40 reanalysis to the observing system: determination of the global atmospheric circulation from reduced observations. *Tellus*, **56A**, 456–471.

Blender, R., & Schubert, M., 2000. Cyclone tracking in different spatial and temporal resolutions. *Monthly Weather Review*, **128**, 377–384.

Compo, G.P., Whitaker, J.S., Sardeshmukh, P.D., Matsui, N., Allan, R.J., Yin, X., Gleason, B.E., Vose, R.S., Rutledge, G., Bessemoulin, P., Brönnimann, S., Brunet, M., Crouthamel, R.I., Grant, A.N., Groisman, P.Y., Jones, P.D., Kruk, M., Kruger, A.C., Marshall, G.J., Maugeri, M., Mok, H.Y., Nordli, Ø., Ross, T.F., Trigo, R.M., Wang, X.L., Woodruff, S.D., & Worley, S.J., in preparation. The Twentieth Century Reanalysis Project. *Quarterly Journal of the Royal Met. Society*.

Déqué, M., Rowell, D.P., Lüthi, D., Giorgi, F., Christensen, J.H., Rockel, B., Jacob, D., Kjellström, E., de Castro, M., & van den Hurk, B., 2007. An intercomparison of regional climate simulations for Europe: assessing uncertainties in model projections. *Climate Dynamics*, **81**(DOI 10.1007/s10584-006-9228-x), 53–70.

Fleagle, R.G., & Businger, J.A., 1980. *An Introduction to Atmospheric Physics*. 2 edn. International Geophysics Series, vol. 25. Orlando: Academic Press.

Gill, A.E., 1982. *Atmosphere-Ocean Dynamics*. International Geophysics series. San Diego, California: Academic Press.

Hanssen-Bauer, I., Drange, H., Førland, E.J., Roald, L.A., Børsheim, K.Y., Hisdal, H., Lawrence, D., Nesje, A., Sandven, S., Sorteberg, A., Sundby, S., Vasskog, K., & Ådlandsvik, B., 2009. *Klima i Norge 2100*. Tech. rept. september 2009. Norsk klimasenter, Oslo.

Haugen, J.E., & Ødegaard, V., 2003. Evaluation of MPI and Hadley simulations with HIRHAM, and sensitivity to integration domains. *Pages 19–29 of:* Iversen, T., & Lystad, M. (eds), *RegClim*. General Technical report, no. 7. http://regclim.met.no/: NILU.

Houghton, J.T., 1991. *The physics of atmospheres*. Cambridge, U.K.: Cambridge University Press.

Ihaka, Ross, & Gentleman, Robert., 1996. R: A Language for Data Analysis and Graphics. *Journal of Computational and Graphical Statistics*, **5**(3), 299–314.

Jones, P.D., 1987. The early twentieth century Arctic high - fact or fiction? *Climate Dynamics*, **1**, 63–75.

Lindzen, Richard S., 1990. *Dynamics in atmospheric physics*. Cambridge, U.K.: Cambridge University Press.

Simmons, A, Uppala, S, Dee, D, & Kobayashi, S., 2007. *ERA-Interim: New ECMWF reanalysis products from 1989 onwards*. ECMWF Newsletter.

Solomon, S., Quin, D., Manning, M., Chen, Z., Marquis, M., Averyt, K.B., Tignotr, M., & Miller, H.L. (eds)., 2007. *Climate Change: The Physical Science Basis. Contribution of Working Group I to the Fourth Assessment Report of the Intergovernmental Panel on Climate Change*. United Kingdom and New York, NY, USA: Cambridge University Press.

van der Linden, P., & Mitchell, J.F.B. (eds)., 2009. *Ensembles: Climate Change and its impacts: summary of research and results from the ENSEMBLES project*. Met Office Hadley Centre, Exeter EX1 3PB, UK: European Comission.

von Storch, H., Langenberg, H., & Feser, F., 2000. A Spectral Nudging Technique for Dynamical Downscaling Purposes. *Monthly Weather Review*, **128**, 3664–3673.

Wern, L., & Bärring, L., 2009. *Sveriges vindklimat 1901-2008 Analys av förändring i geostrofisk vind*. METEOROLOGI Nr 138/2009. SMHI, http://www.smhi.se/sgn0106/if/biblioteket/rapporter_pdf/meteorologi_138v2.pdf.